Seismicity gaps and the shape of the seismic zone in the Banda Sea region from relocated hypocenters

S. Das
Department of Earth Sciences, University of Oxford, Oxford, UK

Received 26 May 2004; revised 27 September 2004; accepted 1 October 2004; published 9 December 2004.

[1] We relocate hypocenters for more than 800 earthquakes deeper than 50 km with $m_b \gtrsim 5.0$, along the Banda arc, using several thousand handpicked direct, depth, and core-reflected phases, in addition to phases reported by the International Seismological Centre. The seismicity distribution is found to be very nonuniform both along the arc and in depth. Gaps in the relocated hypocenters exist along depth in most places of the arc, with the upper edge of the gaps varying from 100 to 450 km depth and the lower edge varying from 350 to 670 km in different portions of the arc. The seismic zone between 129 and 131°E in the 100–200 km depth range is the widest along the arc both in strike and downdip. This region, near the highest arc curvature, has the highest seismic activity and is the only part of the arc with earthquakes continuously occurring from the surface down to below 600 km. The very deep earthquakes under Sulawesi are shown to be part of the west-southwest dipping Seram slab. In the westernmost part of the Banda arc the slab is under downdip tension in the 50–250 km depth range, while the deepest portion of the slab in this region is under compression. From 128 to 131°E the slab between 100 and 200 km depth is under mainly horizontal compression. Our study supports the "two-slab" model for the Banda arc. The depth of the Wadati-Benioff zone below the volcanoes is ~60–100 km for the five volcanoes between 128 and 130°E and ~150 km for the 23 volcanoes between 118 and 124°E. *INDEX TERMS:* 7215 Seismology: Earthquake parameters; 8123 Tectonophysics: Dynamics, seismotectonics; 8164 Tectonophysics: Stresses—crust and lithosphere; 8166 Tectonophysics: Stresses—deep-seated; *KEYWORDS:* Banda Arc seismicity, earthquake relocation, deep earthquakes

Citation: Das, S. (2004), Seismicity gaps and the shape of the seismic zone in the Banda Sea region from relocated hypocenters, *J. Geophys. Res.*, *109*, B12303, doi:10.1029/2004JB003192.

1. Introduction and Motivations for the Study

[2] The arcuate Banda subduction zone, at the intersection region of three major plates, Eurasia, Australia, and Pacific (Figure 1), is one of the most complex tectonic areas in the world. The region is characterized by several subduction zones dipping in different directions in close proximity to one another (Figure 2a). Here the Australian plate subducts northward at a velocity of ~8 cm yr^{-1}. The westward motion of the Pacific plate relative to the Eurasian plate at a velocity of ~9 cm yr^{-1} is accommodated by west-southwestward subduction with a left-lateral component along the Seram Trough [*DeMets et al.*, 1994; *Bock et al.*, 2003]. Near western Timor, the Australian continental shelf started to collide with the island arc around 5 Ma [*Bowin et al.*, 1980]. A recent GPS study by *Genrich et al.* [1996] reports a very low present-day convergence rate normal to Timor (less than 1 cm yr^{-1} today), indicating that active subduction has significantly slowed down due to this continental collision. The seismicity reported by the International Seismological Centre (ISC), deeper than 50 km, and for the period 1962 to September 1996, is shown in map view in Figure 2b.

[3] The Banda subduction zone has one of the highest curvature of any major subduction zone, the ~2200 km long arc curving through an angle of 180° at its eastern portion. This curvature is observable in the seismicity, from the surface all the way down to about ~650 km depth. On the basis of geological and seismological data, *Katili* [1975] proposed that the entire arc was a single subduction zone contorted through 180°, but the details were sketchy. In a seminal paper, *Cardwell and Isacks* [1978] used seismological data to define the geometry of Banda subduction and suggested that the apparent 180° curvature of the Banda arc arises from two adjacent, oppositely dipping subducting plates. One of these is the northward subducting Australian plate beneath Eurasia along the Timor trough that follows the islands of Flores, Timor and Tanimbar (FTT), through Kai. At its easternmost portion, the arc and the associated slab turn northward, believed to be the result of the collision of the Australian plate with Eurasia. The second plate, from Aru to Buru, is the west-southwest (WSW) subducting Pacific plate below Eurasia, along the east-west trending Seram trough [*Cardwell and Isacks*, 1978; *Hamilton*, 1979].

0148-0227/04/2004JB003192$09.00

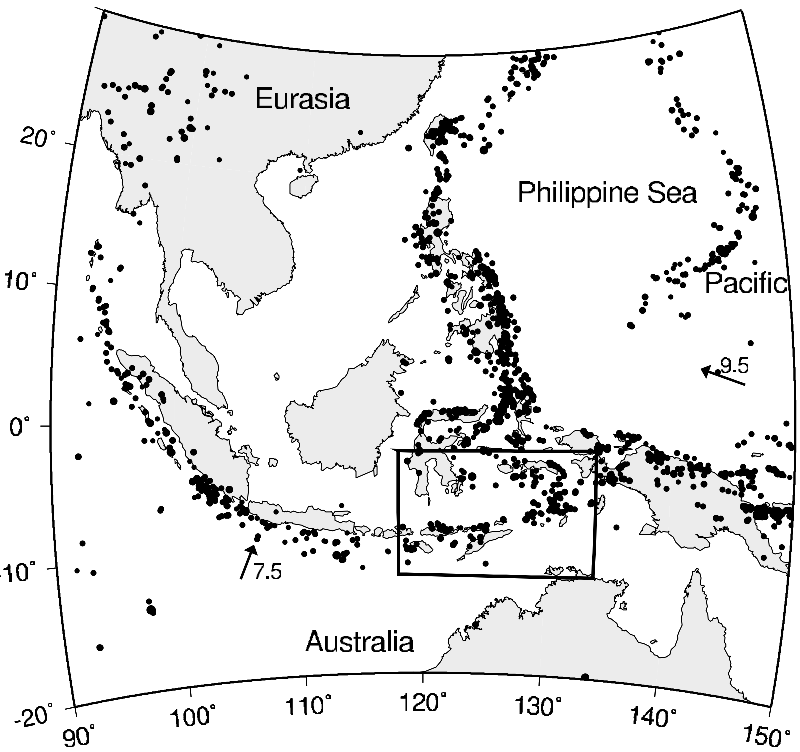

Figure 1. Locations of shallow earthquakes outlining major plates to show the large-scale regional tectonics of the study area. The plate motion vectors for the Australia and Pacific plates relative to Eurasia shown are taken from NUVEL-1A [*DeMets et al.*, 1994], the values being in cm yr^{-1}.

Figure 2b clearly shows that the Seram slab has much lower seismic activity compared to the north subducting Tanimbar portion of the slab. To accommodate the complex tectonic motions of this region, the three major plates have been subdivided into smaller plates [*Hamilton*, 1979]. A structural discontinuity separating the Pacific and Australian plates is clearly visible in the discontinuous gravity lows between the Timor and Seram troughs near Aru (~4.5°S, 133°E) (Figure 2a and *Bowin et al.* [1980]). This discontinuity is the Tarera-Aiduna Fault (TAF), a major left-lateral transform fault, which has well known surface expressions further east in western New Guinea [*Hamilton*, 1979]. In the *Cardwell and Isacks* [1978] model, the Bird's Head is subducting along the Seram trough, while sliding past the Australian plate along the TAF, carrying the Bird's Head westward.

[4] By constructing laboratory models of slabs using resin and plaster, *Yamaoka et al.* [1986] showed that the only way to fit the 180° curvature of the Banda arc seismicity by the contortion of a single slab is to introduce a tear in the slab before it is bent. They placed this tear at ~6°S. *McCaffrey* [1988] and *McCaffrey and Abers* [1991] focused on the tectonics of the shallower portions of the Sunda and Banda arcs. Their earthquake slip vectors clearly show active subduction under Seram, and they concluded that the subduction occurs at a speed

Figure 2. (a) Tectonic setting of the study region and adjacent areas, with gravity field from *Sandwell and Smith* [1997]. Solid arrows indicate plate velocity vectors from NUVEL-1A [*DeMets et al.*, 1994]. Arrows north of the Tarera-Aiduna Fault (TAF) represent the motion of the Pacific plate relative to the Eurasia plate; south of the TAF they indicate the motion of the Australia plate relative to Eurasia, all values being in cm yr^{-1}. WSW subduction of the Bird's Head block beneath the Seram trench, inferred from GPS data [*Bock at al.*, 2003], is shown by the open arrow. Black triangles indicate volcanoes, taken from *Simkin and Siebert* [1994]. Black lines with open triangles show thrust faults, dipping in the direction of the triangles. The black line with harpoons on either side shows the position of the TAF and the direction of relative movement across it [*Hamilton*, 1979]. FT, Flores Thrust; WT, Wetar Thrust; SBB, South Banda Basin; NBB, North Banda Basin; and WB, Weber Deep. (b) Seismicity of the study region for the period 1964–1996. ISC hypocenters with $m_b > 4.5$ for earthquakes deeper than 50 km are shown. Circles are color coded by depth, as shown in the key. The size of circle is proportional to the earthquake magnitude. When considering the many smaller earthquakes seen in the ISC seismicity, it must be kept in mind that it is difficult to obtain accurate magnitudes for earthquakes with $m_b < 5$. Black lines are faults shown in Figure 2a. The deep M_w 7.8 Flores earthquake of 17 June 1996 located at (−7.1, 122.6) at 586 km depth is clearly seen. It was the largest and deepest known earthquake in the entire Sunda and Banda regions. See color version of this figure at back of this issue.

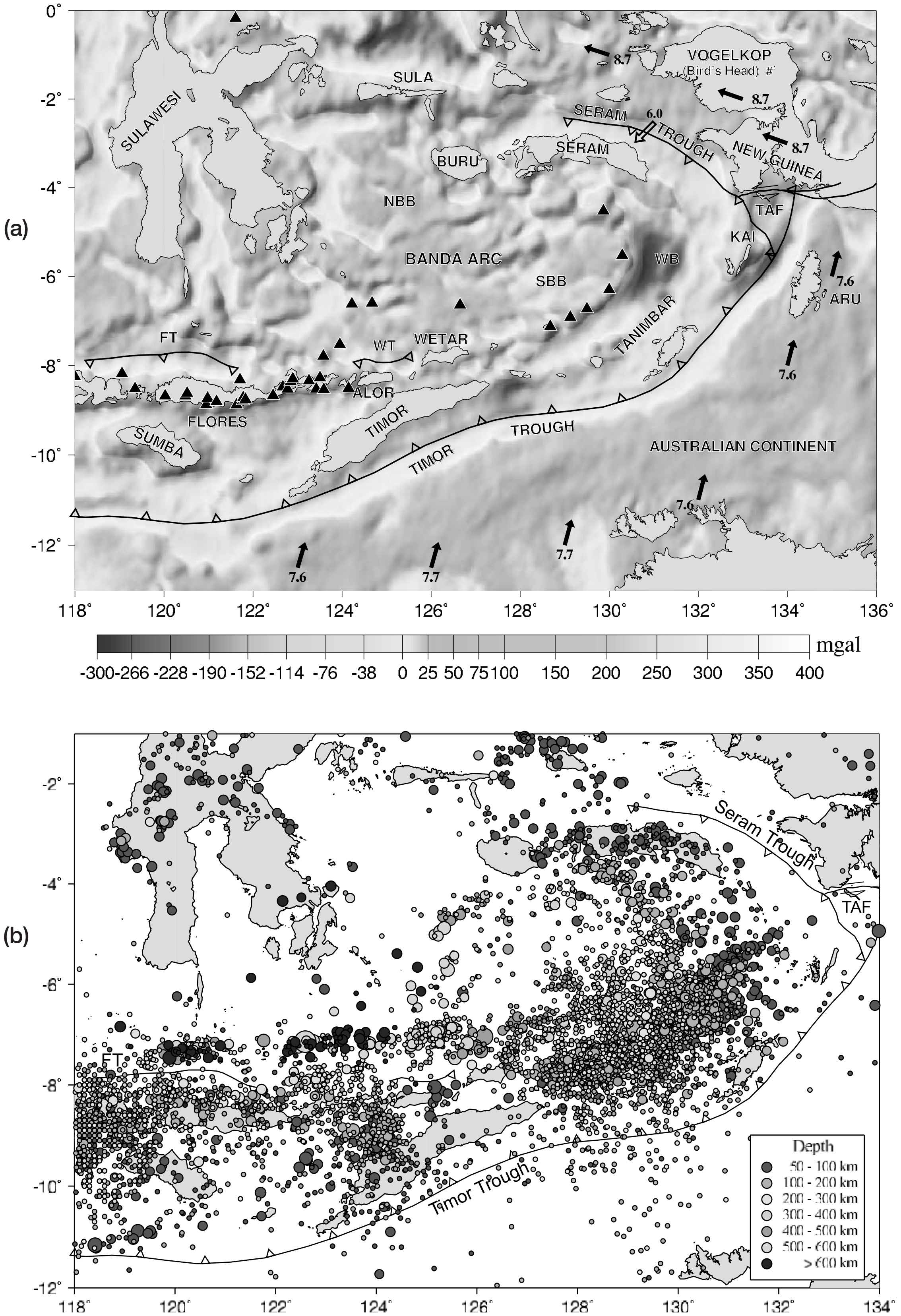

(a)
0°
-2°
-4°
-6°
-8°
-10°
-12°
118°
120°
122°
124°
126°
128°
130°
132°
134°
136°
SULAWESI
SULA
VOGELKOP
(Bird's Head)
8.7
8.7
8.7
6.0
SERAM
TROUGH
SERAM
BURU
NEW GUINEA
NBB
TAF
KAI
BANDA ARC
WB
SBB
7.6
ARU
FT
TANIMBAR
WT
WETAR
7.6
ALOR
FLORES
TIMOR
TROUGH
SUMBA
TIMOR
AUSTRALIAN CONTINENT
7.6
7.7
7.6
7.7
-300
-266
-228
-190
-152
-114
-76
-38
0
25
50
75
100
150
200
250
300
350
400
mgal
(b)
-2°
-4°
-6°
-8°
-10°
-12°
118°
120°
122°
124°
126°
128°
130°
132°
134°
Seram Trough
TAF
FT
Timor Trough
Depth
50 - 100 km
100 - 200 km
200 - 300 km
300 - 400 km
400 - 500 km
500 - 600 km
> 600 km

Figure 2

of about 6 cm yr^{-1}, a rate confirmed by recent GPS measurements [*Bock et al.*, 2003]. By considering the kinematics of plate motion, *McCaffrey* [1988, p. 15,163] concluded that "it is geometrically incompatible" for the Australian plate to subduct "simultaneously beneath both the Timor and Seram troughs" and, on the basis of the lack of evidence for extension between Sumba and Seram, [p. 15,177] that the "single-plate hypothesis is unlikely." *Bowin et al.* [1980] showed geological evidence for the presence of the Australian shelf all around the outer Banda arc, in the southeast of Sulawesi, on Buru, and northeast of Seram. This observation could support the hypothesis of a single zone contorted by 180°. However, the presence of Australian shelf to the north of the northern limb of the Banda zone has been explained by *McCaffrey and Abers* [1991] as being due to left-lateral movement along the TAF, which has transported the northern portion of the Australian shelf westward. Recent tomographic images of the region [*Widiyantoro and van der Hilst*, 1997] clearly show the "spoon shape" of the slab under Banda, as seen from the seismicity in Figure 2b. However, when discussing *Cardwell and Isacks*'s [1978] two-slab model, *Widiyantoro and van der Hilst* [1997, pp. 176–178] state "our inversions cannot resolve such detail."

[5] *Hamilton* [1979] first described this region as "tangled." Yet, two decades later, *Widiyantoro and van der Hilst* [1997, p. 173] wrote that "despite numerous studies of the Banda region, .., there is no consensus on the complicated structure beneath the Banda region". Most recently, *Bird* [2003, paragraph [43]] has described this region as having "the most complex neotectonics on Earth." Untangling the complexity of the Banda arc is the main motivation for us to reexamine this region. *Cardwell and Isacks* [1978] used ISC located earthquake hypocenters all the way to the deepest parts of the seismic zone, for the period 1959 to 1973, and first-motion fault plane solutions in their study. *McCaffrey* [1988] used ISC hypocenters to ~100 km depth, available Harvard centroid moment tensor (CMT) solutions, and modeled *P* and *SH* waveforms from the World-Wide Standardized Seismograph Network (WWSSN) and some Global Digital Seismic network (GDSN) stations for earthquakes between 1962 and 1984. Recent studies by us in the adjacent Sunda region to the west [*Schöffel and Das*, 1999; *Das and Schöffel*, 2000; *Das et al.*, 2000] showed that relocating the earthquakes accurately allows one to see details not seen before. In that study of the Sunda arc, thousands of additional phases (*pP*, *sP*, *PcP*, *ScP*) not reported by the ISC were handpicked and used to relocate the earthquakes, using the method of joint hypocenter determination (JHD). Comparisons of their locations and errors with those from other catalogs are detailed in *Schöffel and Das* [1999] and *Das and Schöffel* [2000]. It was demonstrated that as the locations are improved, the seismic zone gets narrower and narrower (even when the number of earthquakes is larger) defining a very clear shape. Under Sunda, it was found that the slab is contorted along strike and, below about 500 km in one region, actually bends antithetically to its direction of subduction at the surface. Using the relocated hypocenters together with centroid moment tensor solutions, they proposed their "slab-shattering" model, in which the Sunda slab thickens, shortens and weakens by shearing along conjugate faults on the upper and lower portions of the Wadati-Benioff zone (WBZ), before penetrating below 670 km [*Das et al.*, 2000]. The reliability of the locations permitted differentiation between earthquakes on the upper and lower sides of the seismic zone. The earthquakes toward the lower surface of the seismic zone were generally found to be fewer and smaller than those in the central and upper portions, with most of the total moment being due to earthquakes on the upper side. Implications for thermal models of the slab were discussed by *Das and Schöffel* [2000]. The success of our Sunda arc study encouraged us to pursue the present study. Moreover, the information obtained in this study is essential for reliable reconstructions of the tectonic histories of complex regions, for a better understanding of the past and current tectonics and plate driving forces such as the existence of basal shear traction below plates, as well as to identify the distribution of lithospheric material in the upper mantle.

1.1. Deep Sulawesi Earthquakes

[6] The isolated, deep earthquakes under Sulawesi (Figure 2b) lie ~250–300 km to the north of the deepest part of the Flores-Timor seismic zone. *Cardwell and Isacks* [1978] and *Lundgren and Giardini* [1994] connected these earthquakes to the FTT, by requiring the slab to be flat and continuous for ~250–300 km at the depth of about 600 km. However, Figure 2b shows there are very few earthquakes at the depths where this slab would be expected to lie horizontally. Thus a final motivation for this study was to see whether or not there are truly any earthquakes in this region at this depth, or whether the deep Sulawesi earthquakes are connected to the FTT at all. A sharp 90° bend in the seismic zone at depth of about 600 km would be required for this connection. Such a bend would generate large stresses in the slab, and may normally be expected to result in increased seismic activity.

1.2. Depth of the Seismic Zone Below Arc Volcanoes

[7] Though it was accepted for a long time that the depth of slabs below volcanoes was relatively constant from arc to arc, *England et al.* [2003] have shown that this is not true. These authors have taken the depth of the earthquake hypocenters below volcanoes as a proxy for the depth of the slab. For arcs worldwide, they measured this depth using the hypocentral locations of *Engdahl et al.* [1998]. They have found that the depth varies from 65 km to 130 km along different arcs. Our study area had not been included in their study. Since there are more than 30 active volcanoes in this region (Figure 2a), we can accurately measure the depth of the WBZ below these volcanoes from our hypocentral locations.

1.3. Main Aims of the Study

[8] Some of the specific questions we would like to answer regarding the curved Banda arc are the following: (1) At what depths are different parts of the subduction zone seismically active? (2) Does the reliably relocated seismicity over a period exceeding three decades allow us

to distinguish between the one-plate and the two-plate models? (3) How do the deep earthquakes north of the Flores-Timor-Tanimbar WBZ relate to it, and to the deep Sulawesi earthquakes further north? (4) Does the depth of the WBZ below arc volcanoes vary along the Banda arc?

2. Data and Method

[9] The tectonics of the shallow parts of the Banda arc have been discussed in detail in earlier studies by *Hamilton* [1979], *McCaffrey* [1988], and *McCaffrey and Abers* [1991] [see also *Bird*, 2003], which also discuss the tectonic history of the region. Here, we shall concentrate only on the parts of the subduction zone deeper than 50 km. The procedure of *Schöffel and Das* [1999], which we shall follow, is particularly suited for the relocation of such earthquakes. Since subcrustal earthquakes can occur only inside subducting plates [see, e.g., *Kirby et al.*, 1996b], the positions of the earthquakes define the minimum spatial extent of the slab. Thus our approach does not find the shape of the slab but only a very detailed picture of the seismic part of the slab. We shall use a much larger seismological data set than has been used in previous studies to obtain a clearer picture of the WBZ below Banda. We shall then combine this with all available Harvard CMT solutions [*Dziewonski et al.*, 1983–1999] for our interpretations.

[10] Very accurate hypocentral locations are essential to answer the questions we have posed. *Pegler et al.* [1995], *Pegler and Das* [1996, 1998] and *Schöffel and Das* [1999] have clearly demonstrated that the earthquake hypocentral locations provided by agencies such as the International Seismological Centre (ISC) are not sufficiently reliable for such purposes, though previous studies giving an overall picture of this region have been carried out using such data [*Cardwell and Isacks*, 1978; *McCaffrey*, 1988; *McCaffrey and Abers*, 1991]. Body waveform studies provide another constraint on earthquake positions, although they only allow the study of the larger earthquakes that have been recorded by a sufficient number of stations. For our relocations, ISC locations for the period from 1962 to September 1996 were used as primary locations. We attempt to relocate all earthquakes in this period reported by ISC with body wave magnitude $m_b \geq 4.5$ in the depths range between 50 and 400 km. For earthquakes deeper than 400 km, we attempt to relocate all reported earthquakes in the same time period. Earthquakes with less than 10 available *P* phases are discarded. We use the joint hypocenter determination (JHD) algorithm [*Dewey*, 1971, 1983], with some minor modifications, described by *Schöffel and Das* [1999] and *Henry and Das* [2001]. We handpicked 1398 *P*, 746 *S*, 564 *pP*, 434 *sP*, 526 *PcP* and 494 *ScP* phases from the Global Digital Network of broadband or short-period seismograms from beginning of August 1975 to end of September 1996. This was supplemented by ISC reported phases. The very significant improvement achieved by adding extra phases to the JHD relocation [*Schöffel and Das*, 1999] is due to the presence of the core-reflected phases (*PcP* and *ScP*) that are seldom reported by agencies. For earthquakes below ~200 km hypocentral depths, these are large in amplitude and very impulsive at many epicentral ranges, in contrast to the more widely used depth phases, whose arrival times are difficult to pick [*Schöffel and Das*, 1999; *Das and Schöffel*, 2000]. The comparison of the relocated hypocenters with other catalogs is very similar to those plotted in map and profile views for the Sunda region in *Schöffel and Das* [1999] and *Das and Schöffel* [2000], and the reader is referred to these papers for the comparison.

[11] We consider earthquakes to be "reliably" relocated only when the largest semiaxes ℓ_1 of the 90% confidence error ellipsoid [*Dewey*, 1971, 1983] is $\leq$30 km, and our interpretations will be based primarily on these earthquakes. Occasionally, earthquakes with somewhat larger error may be included in the discussion (it is always clear from the context and from the captions for Figures 6a–6d in section 3 when this is done). In general, we almost always successfully relocate earthquakes with $m_b > 5$, and there are very few earthquakes that have CMT solutions but cannot be reliably relocated. We also find that the error ellipsoids are usually larger for smaller earthquakes and pre-1964 earthquakes. The errors in the horizontal directions are many times smaller than that in the vertical direction, so that the longest axis of the error ellipsoid is always nearly vertical. (This will be seen in Figure 9 in section 4.3, where we show one vertical profile which includes the error ellipses.) Of 2273 reported earthquakes with $m_b > 4.5$, 1105 have $m_b > 5.0$ and 847 were relocated by us with $\ell_1 \leq 30$ km, of which 677 had $\ell_1 \leq 20$ km and 277 had $\ell_1 \leq 10$ km.

3. Distribution of Relocated Earthquakes

[12] The reliably relocated seismicity of the Banda arc region obtained in this study is shown in map view in Figure 3a and in three-dimensional (3-D) perspective plots looking from two different directions in Figure 3b. The region from 118 to 125°E overlaps the eastern part of the arc studied by *Schöffel and Das* [1999]. Figure 4 shows the available CMT solutions in the top 50 km, and Figure 5 shows those below 50 km depth. The earthquakes are also shown in 18 vertical profiles in Figures 6a–6d, with the locations of the profiles shown in Figure 3a. The sections are perpen-

Figure 3. (a) Map view of the relocated seismicity deeper than 50 km and with relocation error less than 30 km. Same color coding as in Figure 2b. Two CMT earthquakes from *Dziewonski et al.* [1983–1999] and *Huang et al.* [1997] are shown under southeast Sulawesi. Boxes show the positions of the profiles to be used in Figures 6a–6d. Solid black lines are faults, and the black triangles are volcanoes, as shown in Figure 2a. The dashed black line on the eastern part of the arc will be discussed in section 4.2. Arrows outside the frame show directions from which perspective plots are shown in Figure 3b. (b) (top) Perspective plots of the relocated seismicity, seen from two directions, 15° west of south and 5° north of east. (bottom) Seismicity on the FTT and Seram slabs, obtained by plotting earthquakes to the south and north of the 5°S latitude line. (This may not have separated the deep earthquakes where the slabs merge.) Colors, symbols, etc., are the same as in Figures 2b and 3a. See color version of this figure at back of this issue.

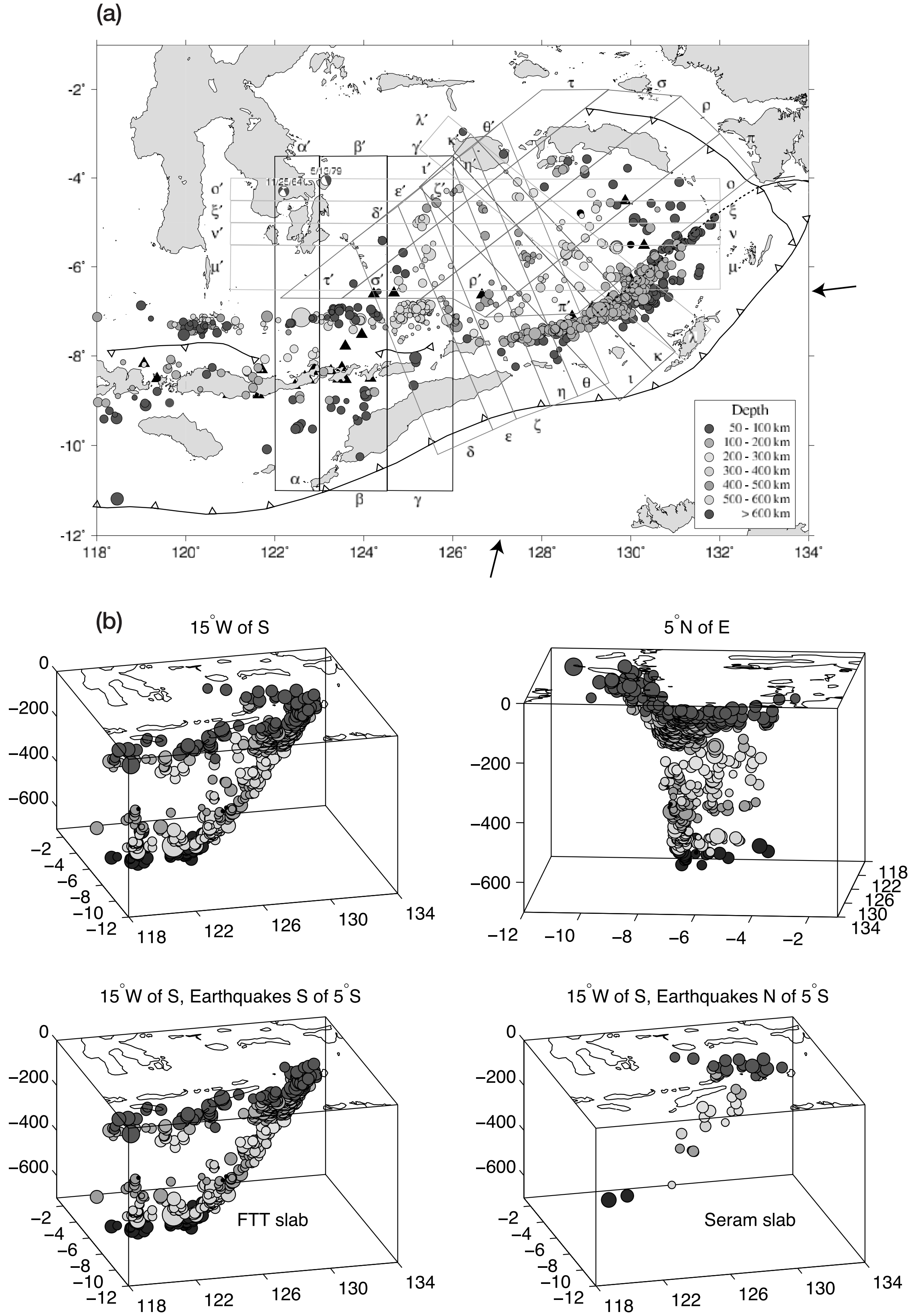
(a)
Depth
50 - 100 km
100 - 200 km
200 - 300 km
300 - 400 km
400 - 500 km
500 - 600 km
> 600 km
(b)
15° W of S
5° N of E
15° W of S, Earthquakes S of 5° S
15° W of S, Earthquakes N of 5° S
FTT slab
Seram slab

Figure 3

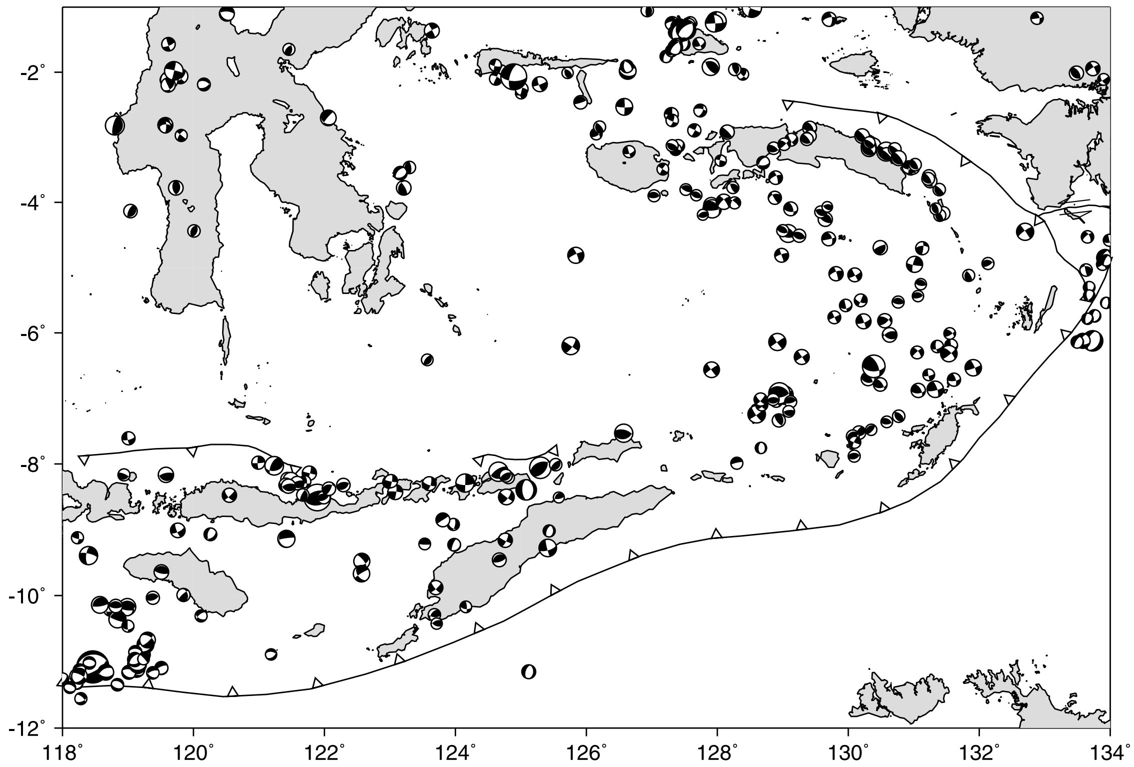

Figure 4. CMT focal mechanisms in the study area (plotted at the CMT location) in the depth range 0–50 km.

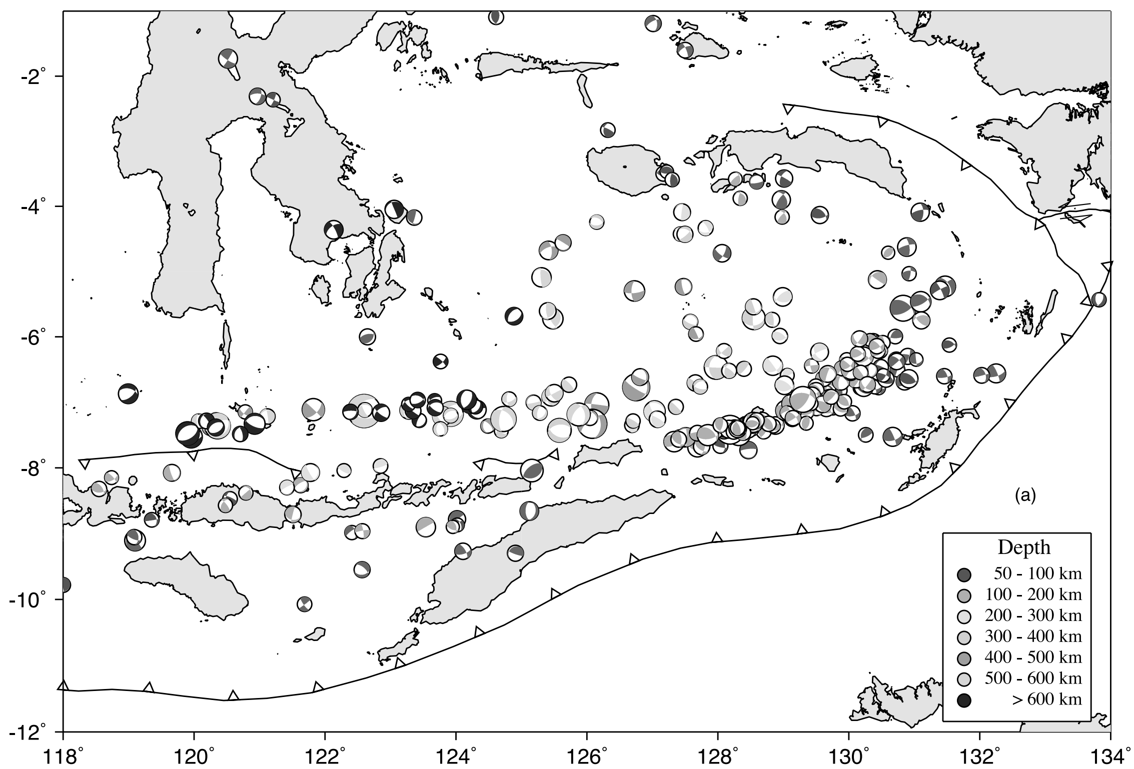

Figure 5. Same as Figure 4 but for earthquakes deeper than 50 km. CMTs are plotted at their relocated positions. The same color coding with depth as Figure 2b is used. See color version of this figure at back of this issue.

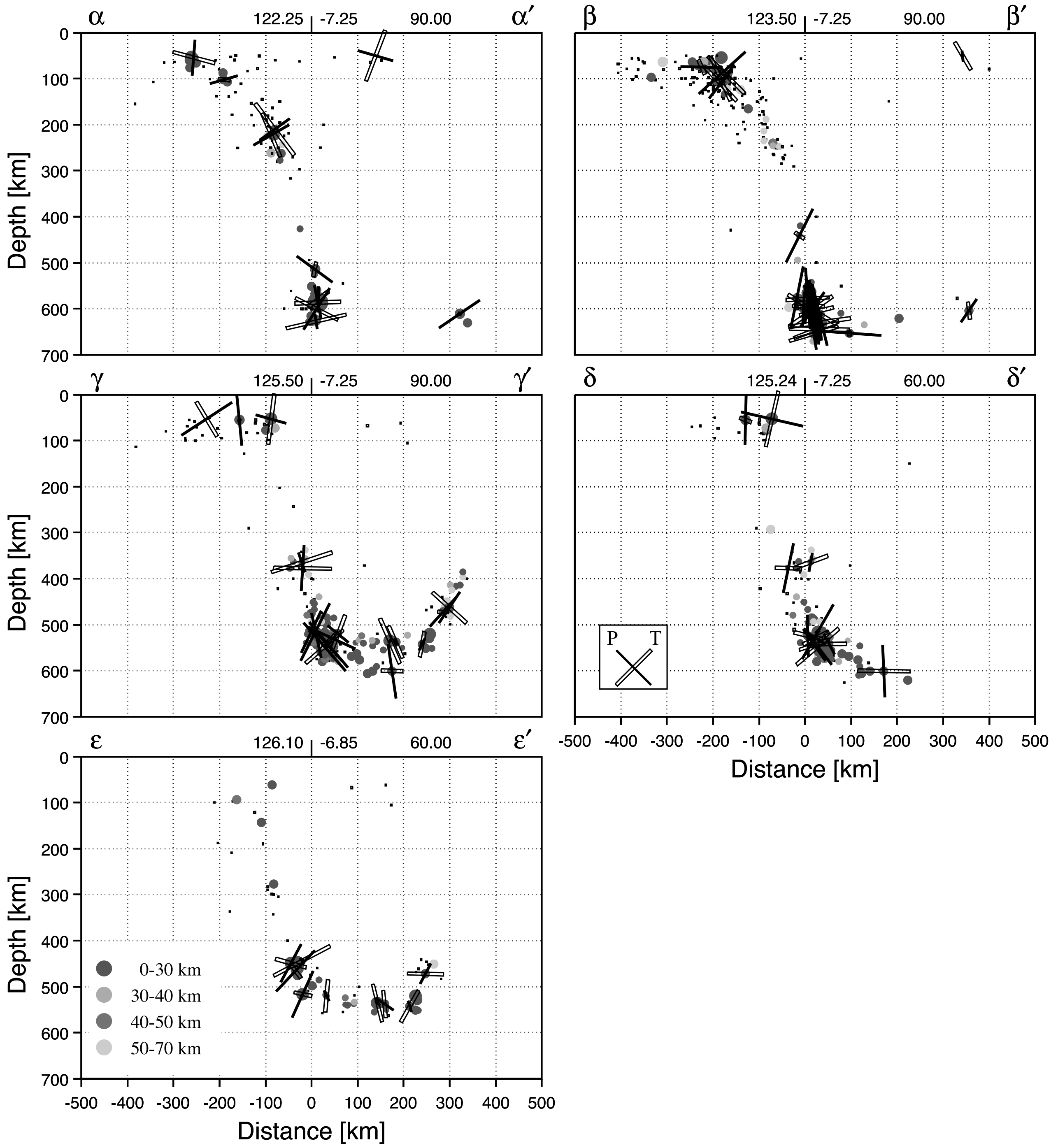

Figure 6a. Relocated seismicity profiles αα′ to ϵϵ′ (locations indicated in Figure 3a), projected onto the center line of the profile. Center position (longitude, latitude) and azimuth of the projection (e.g., 90° indicates profile is looked at from the east) are given on the top of each profile. The *P* and *T* axes of the CMT solution [*Dziewonski et al.*, 1983–1999; *Huang et al.*, 1997] are also shown. The different colored circles represent different maximum errors in the relocation, as shown in the color key. The *P* and *T* axes are projected into the plane of the profile and plotted at their relocated positions. Small open squares show the ISC seismicity with $m_b > 4.0$, which either could not be relocated or had a relocation error greater than 70 km. Symbols used for the *P* and *T* axes are shown. See color version of this figure at back of this issue.

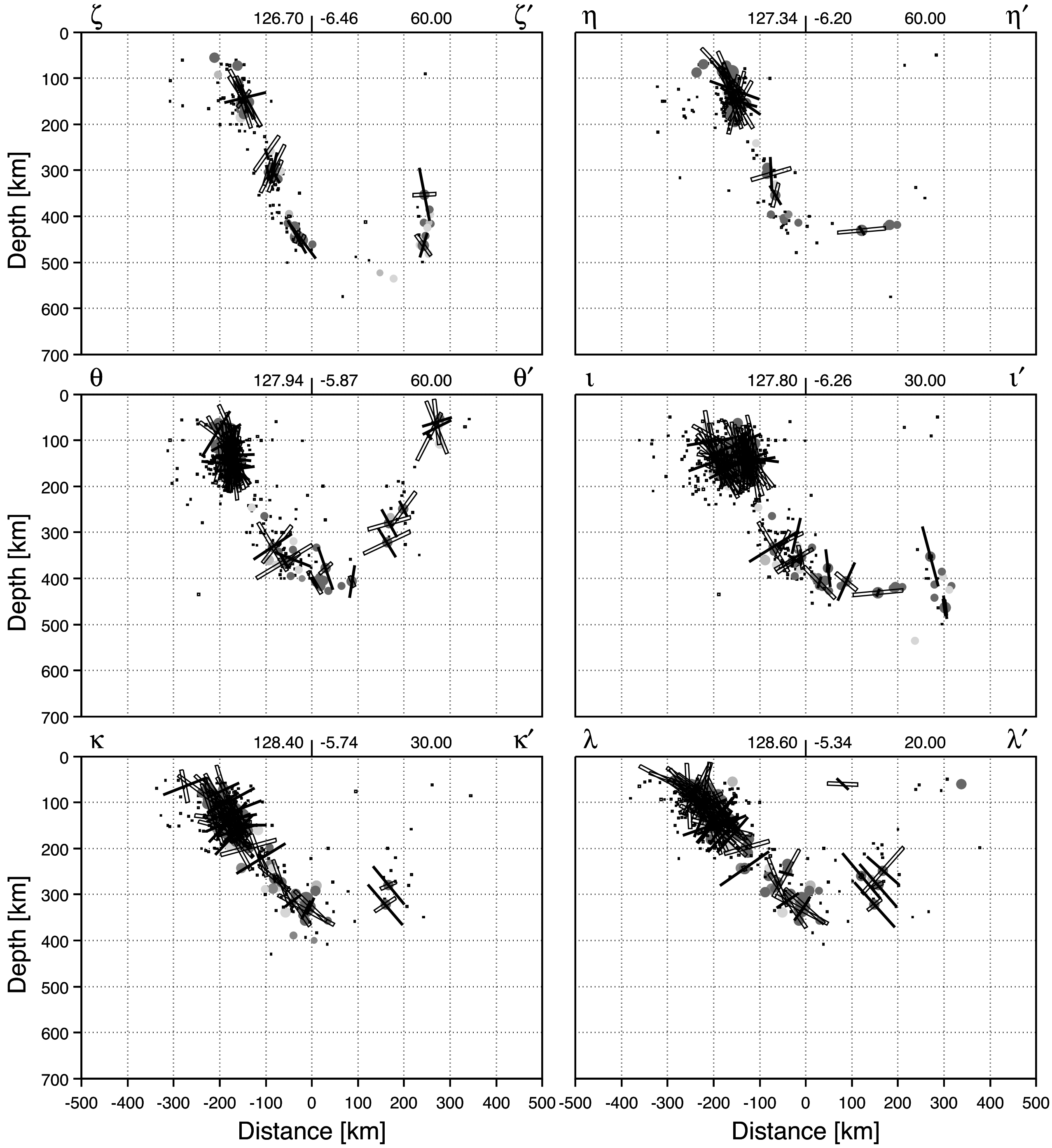

Figure 6b. Same as Figure 6a but for profiles ζζ′ to λλ′. See color version of this figure at back of this issue.

dicular to the trend of the intermediate depth seismicity or the outer trench and are deliberately chosen to be narrow to reveal details. We shall use the term "gap" to mean regions of fewer and smaller earthquakes, rather than regions of no seismicity at all. Thus a "gap" is a gap in the reliably relocated hypocenters.

3.1. Comparison of the ISC Data With Our Relocated Hypocenters

[13] The most prominent difference between the ISC and the relocated hypocenters is the marked decrease in the number of moderate to large earthquakes. Since the reliably relocated hypocenters are always for the larger earthquakes, usually $m_b > 5.0$, these earthquakes give a rather different impression of the seismicity of the Banda arc than that from the ISC data. Since the hypocenters move after relocation, simply plotting the larger ISC earthquakes does not lead to exactly the same distribution as would be obtained by plotting those same earthquakes at their relocated positions.

[14] The curved seismic zone, closely following the island arcs, is clearly defined by both the ISC seismicity

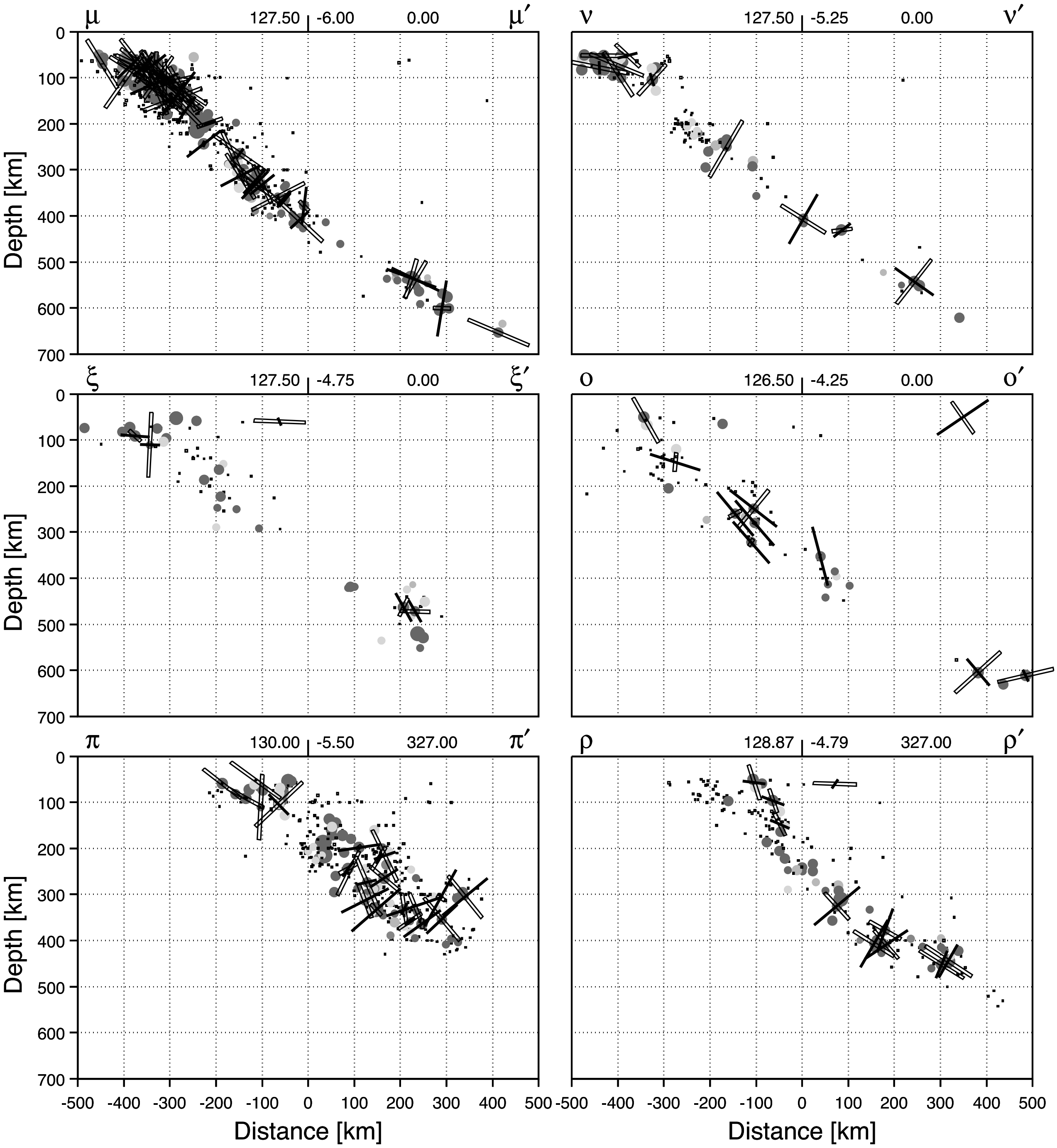

Figure 6c. Same as Figure 6a but for profiles μμ′ to ρρ′. See color version of this figure at back of this issue.

and the relocated seismicity, and both data sets show that the seismicity is distributed very nonuniformly along the arc as well as in depth. The ISC data in Figure 2b show clusters of larger earthquakes near longitudes 118–120°E, 123–124°E and 127–132°E. In the first two regions, these clusters disappear in the relocated data (Figures 3a and 3b). The variability of seismicity along the arc from 118 to 127°E still exists but is now less pronounced. The seismicity around 124°E retains its elongated shape normal to the arc. Such linear zones across the trench were interpreted by *Schöffel and Das* [1999] as being due to nearly parallel subducted transform faults that are still active. *Kirby et al.* [1996a] noted similar linear zones in the Nazca subduction zone.

3.2. Seismicity Distribution Along Slab Depth

[15] The relocated hypocenters show that the dip of the WBZ is highly variable along the Banda arc, as was noted by *Cardwell and Isacks* [1978, Figure 4]. The region between Timor and Aru (127–132°E) at 100–

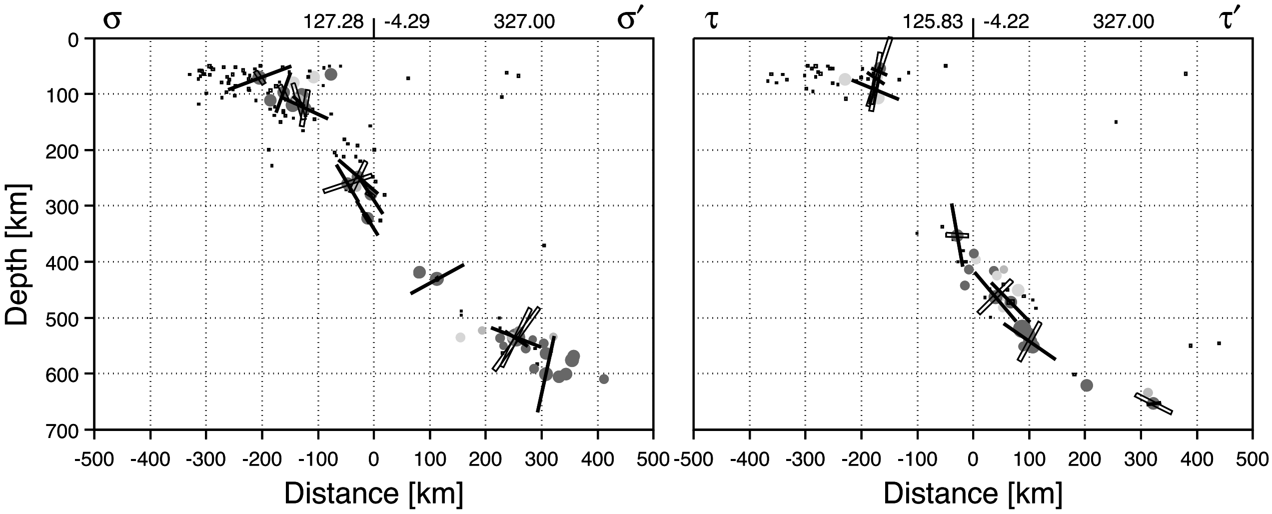

Figure 6d. Same as Figure 6a but for profiles σσ′ and ττ′. See color version of this figure at back of this issue.

200 km depths has the highest seismicity along the entire arc, both in the Indonesia and Banda regions, in both data sets, as well as the largest concentration of CMT mechanisms (Figure 5). This depth range is seen to be seismically very quiet in the adjacent regions on both sides along the arc. Some of these features are not as clear in earlier studies of this region [e.g., *Cardwell and Isacks* [1978]; *McCaffrey*, 1988], showing that examination of reliably relocated seismicity over a longer time period is worthwhile.

[16] The seismic zone between Timor and Tanimbar in the 50–200 km depth range shows a gentle northeasterly turn in the 128–130°E longitude range. However, as we move deeper, the curvature to the north occurs further and further to the west, and increases with depth, with the trend of the 500–600 km deep earthquakes showing a turn of almost 90° to the north near 125°E. In the region of this curvature (between 125 and 131°E), the horizontal width of the seismicity at different depth levels (as indicated by the color coding) increases, implying that the dip of the seismic zone decreases with depth.

[17] As we follow the seismic zone north of the approximate westward extrapolation of the TAF (Figures 3a, 3b, 4, and 5), we see a very abrupt change in the trend of the seismicity at all depths. This is the Seram subduction zone which extends from Aru to Buru, has a northwesterly trend, and dips to the WSW. The island arc of the Seram zone has a curvature similar to that of the island arc of the FTT zone, but the seismic zone is less curved. The seismic zone behaves differently at the two bends. On the FTT, it is continuous around the bend to the north, but at the second sharper bend of the arc to the west, a much larger change in the WBZ is seen. This is why the continuity of the slab around the first bend has never been controversial, but that around the second bend has. No zone of very high seismicity, comparable to that seen in 100–200 km depth range between Timor and Aru, is seen in the Seram zone.

3.3. Seismicity Gaps Along Slab Depth

[18] One of the most prominent features of Figure 3b is the lack of seismicity at some depths along the arc. The lack of earthquakes at depths around 300–400 km in many subduction zones worldwide is well known [*Kirby et al.*, 1996a, 1996b]. *Kirby et al.* [1996b] also noted the absence of earthquakes between 350 and 500 km depths from 107 to 115°E in the ISC hypocenters, further west of our study region. *Estabrook* [2004] plotted both the number of earthquakes and the cumulative seismic moments for small and large earthquakes occurring in the period 1977–1998 as a function of depth for the Indonesian, and other, slabs. For Indonesia, he showed that the 200–500 km depth range has remarkably few earthquakes and low cumulative seismic moment. What is striking in our study is the extreme variability of the depths of the upper and lower edges of the gap along the same arc (Table 1). *Kirby et al.* [1996b] showed that the maximum depth of seismicity in a slab increases with increasing thermal parameter (the product of plate age entering trench and vertical descent rate). Along the Indonesian arc, the age of the lithosphere and the convergence rate increase from west to east, and deep earthquake start occurring abruptly as we move from west to east as the thermal parameter exceeds about 5000. This, and similar observations worldwide, provided an observational basis for the thermokinetic models of deep earthquake mechanism [*Kirby et al.*, 1996b]. The fact that in our detailed study of the Banda region we do not find any obvious correlation between the age of the subducting lithosphere, its subduction rate, and the dip of the subduction zone with the depth range of this gap, suggests that other effects, such as increased stresses due to slab contortion and flexure, which in turn affect the thermal regime in the slab, may influence the mechanism by which intermediate and deep earthquakes occur. (See *Estabrook* [2004] for a comprehensive discussion of such mechanisms and related references.)

[19] There are very few earthquakes between 300 and 500 km depths for most of the arc, except around 125–129°E. This latter region is the only part of the entire arc for which earthquakes exist nearly continuously all the way from the surface to its deepest portion around 670 km, seen clearly in profiles μμ′ and νν′ (Figure 6c).

Table 1. Seismicity Gaps

Profile	Gap Depth, km
$\alpha\alpha'$	~300–400
$\beta\beta'$	~300–400
$\gamma\gamma'$	~100–350
$\delta\delta'$	~100–350
$\epsilon\epsilon'$	~300–450
$\zeta\zeta'$	~500–670
$\eta\eta'$	~450–670
$\theta\theta'$	~450–670
$\iota\iota'$	~500–670
$\kappa\kappa'$	~400–670
$\lambda\lambda'$	~400–670
$\mu\mu'$	no gap
$\nu\nu'$	~450–550
$\xi\xi'$	~300–400
oo'	~450–600
$\pi\pi'$	~400–670
$\rho\rho'$	~450–670
$\sigma\sigma'$	~320–420
$\tau\tau'$	no large gap

From 120 to 122°E, there is also a seismicity gap in the 100–300 km depth range on the FTT slab. In the east Timor/Tanimbar zone, there are very few earthquakes between about 125 and 127°E from the surface down to about 400 km, whereas between about 127 and 130°E the gap exists down to about 100 km.

3.4. Stresses in the Slab

[20] The compressional (*P*) and tensional (*T*) axes obtained from the CMT mechanisms are shown in profiles down to 670 km in Figures 6a–6d and in different depth ranges in Figures 7a–7c. The *P* and *T* axes are plotted at their relocated positions. In the 100–200 km depth range (Figure 7a), the compressional axes from 128 to 131°E show two different orientations. They are mostly aligned with the local strike of the seismic zone with some being perpendicular to it, indicating that this region is under mainly horizontal compression. Along the arc, north of the TAF, the shallower *P* axes are perpendicular to the Seram zone, along the local direction of subduction. *Cardwell and Isacks* [1978] attributed the thrust focal mechanisms in western Seram to shallow underthrusting of New Guinea under Seram. In eastern Seram, thrust earthquakes are seen shallower than 50 km (Figure 4), but no earthquakes with CMT mechanisms exist deeper than 50 km. No underthrusting earthquakes are seen under Buru. Along the entire arc, we do not see any unusual "slab push" (downdip compression) earthquakes at shallow depths, as was reported by *Lemoine et al.* [2002] in the Mexican, Chilean, and Peruvian subduction zones.

[21] Two earthquakes (25 November 1964 and 13 May 1979) are reported under southwest Sulawesi below 600 km depth by the ISC, the Harvard CMT catalogue and by *Huang et al.* [1997]. The surrounding region, both in lateral extent in all directions as well as in depth, shows no seismicity for a few hundred kilometers. The CMT location of the more recent earthquake is close to that obtained by the ISC. These earthquakes have been relocated by us, but due to their isolation and their small number, the applicability of the JHD method to them can be questioned. *Engdahl et al.* [1998] relocated these earthquakes and found essentially the same positions. What is important is that these deep Sulawesi earthquakes are consistent in different catalogues, and there is no evidence that they are seriously mislocated.

[22] We find that in the two westernmost profiles $\alpha\alpha'$ and $\beta\beta'$ (Figure 6a), the *T* axes align with the WBZ in the 50–250 km depth range, and the *P* axes lie along the WBZ in the 500–650 km portion, as discussed in *Schöffel and Das* [1999]. Thus, in this region we have the classic behavior for a subducting slab [*Isacks and Molnar*, 1971]. As we move eastward along the arc, this behavior becomes far less consistent (profiles $\epsilon\epsilon'$ to $\lambda\lambda'$ (Figures 6a and 6b), and the seismicity forms a U shape, composed of the north dipping FTT slab and the WSW dipping Seram slab, with seismicity seen at least down to 500 km depth. The clear U shape then disappears from profiles $\mu\mu'$ to $\rho\rho'$ (Figure 6c), as we move eastward around the arc. The variability of the thickness of the WBZ along the arc, seen in Figures 3a and 4, is again clearly seen in the profiles. As under Sunda, the earthquakes in many profiles can be recognized as lying on the upper or lower side of the WBZ (the error ellipses are not plotted but are similar in size to those shown by *Schöffel and Das* [1999], *Das and Schöffel* [2000] and are shown for one profile in Figure 9 in section 4.3). The most interesting fact in Sunda was that the larger earthquakes occurred on the upper side of the slab, but this behavior is not found here. A remarkable uniformity of the CMT mechanisms on the upper and lower sides of the Sunda slab was seen when the mechanisms were plotted after being rotated into the vertical plane through the slab [*Das et al.*, 2000]. For the Banda region, such an uniformity exists (plots not shown) at the part of this arc adjacent to Sunda (that is profiles $\alpha\alpha'$ and $\beta\beta'$), but disappears further eastward along the arc, suggesting that the stress regime is more complex toward the east.

4. Discussion

4.1. Shape of the Banda Arc Wadati-Benioff Zone

[23] In the eastern Flores and the western Timor portion of the arc, the WBZ extends to below 600 km, with a clear gap starting at intermediate depths and extending to different depths in the different profiles $\alpha\alpha'$ – $\gamma\gamma'$ (Figure 6a). Along $\alpha\alpha'$, the WBZ near 600 km is thicker than that near 400 km, as seen in *Schöffel and Das* [1999] and *Das et al.* [2000] under Sunda. The change in the thickness of the WBZ suggests a change in the thickness of the slab itself with depth. In the region of profile $\gamma\gamma'$ (Figure 3a), we see that the WBZ between 500 and 600 km depth is almost twice as thick as the regions to its east and west. This may suggest a piling up of the slab as it descends into the mantle. In the region between about 129 and 131°E, we have a seismic zone that is much thicker in the 100–200 km depth range than the zones at comparable depths on either side of it. We suggest that this is either due to a folding of the WBZ as it curves around the arc (like the fold of a hanging curtain) or due to the presence of the second slab, the Seram slab, in close proximity to the FTT slab.

[24] Along profile $\beta\beta'$ (Figure 6a), the earthquakes lying from 100 to 350 km to the right of the center line of the profile below 600 km depth indicate a slab flattening as it

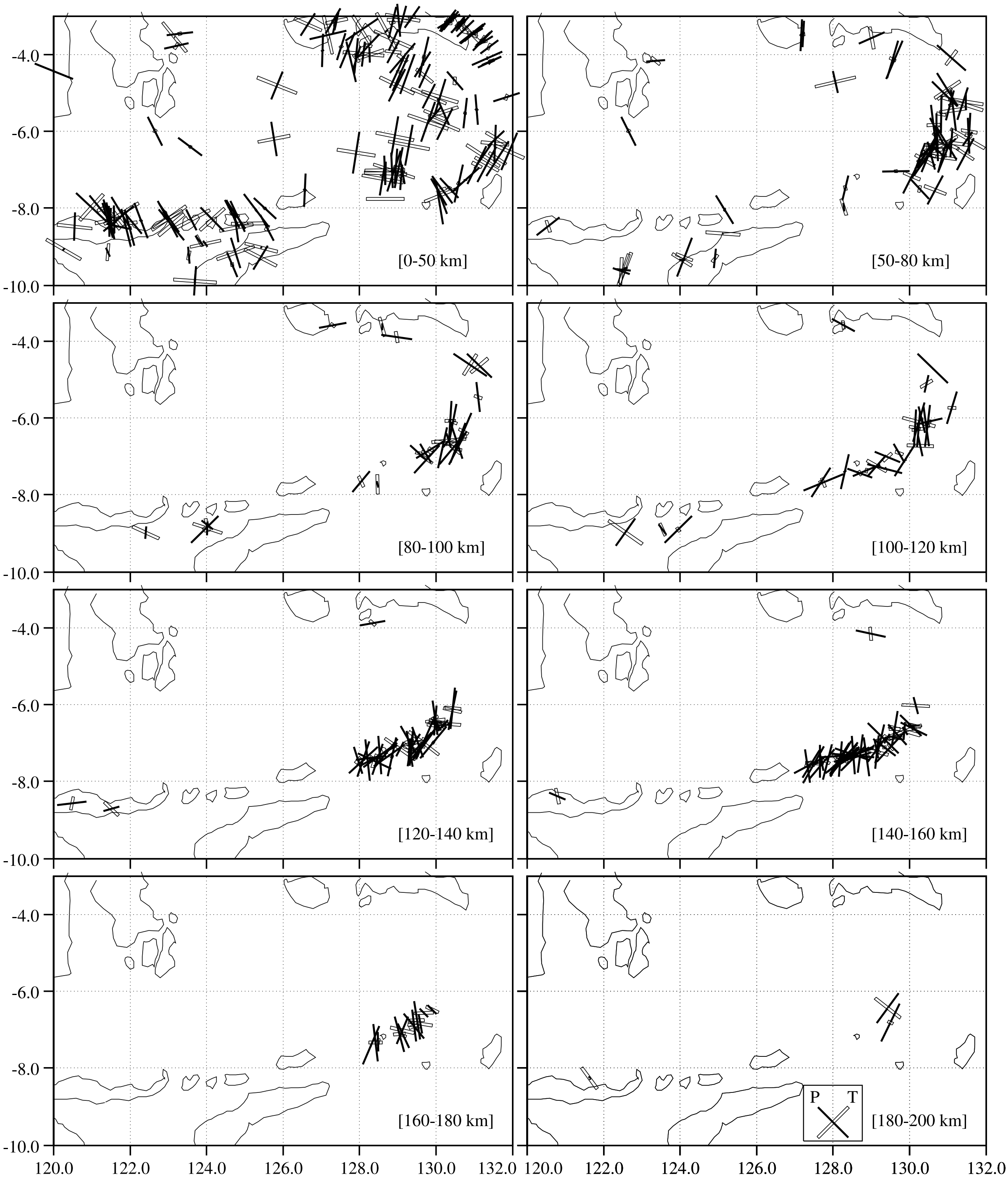

Figure 7a. Map view of the study area showing the *P* axes and *T* axes obtained from CMT mechanisms, in depth sections from the surface down to 200 km depth. Symbols for the axes are shown in the inset, which also gives the maximum length of the axes for pure horizontal compression and tension (a shorter axes indicate a vertical component).

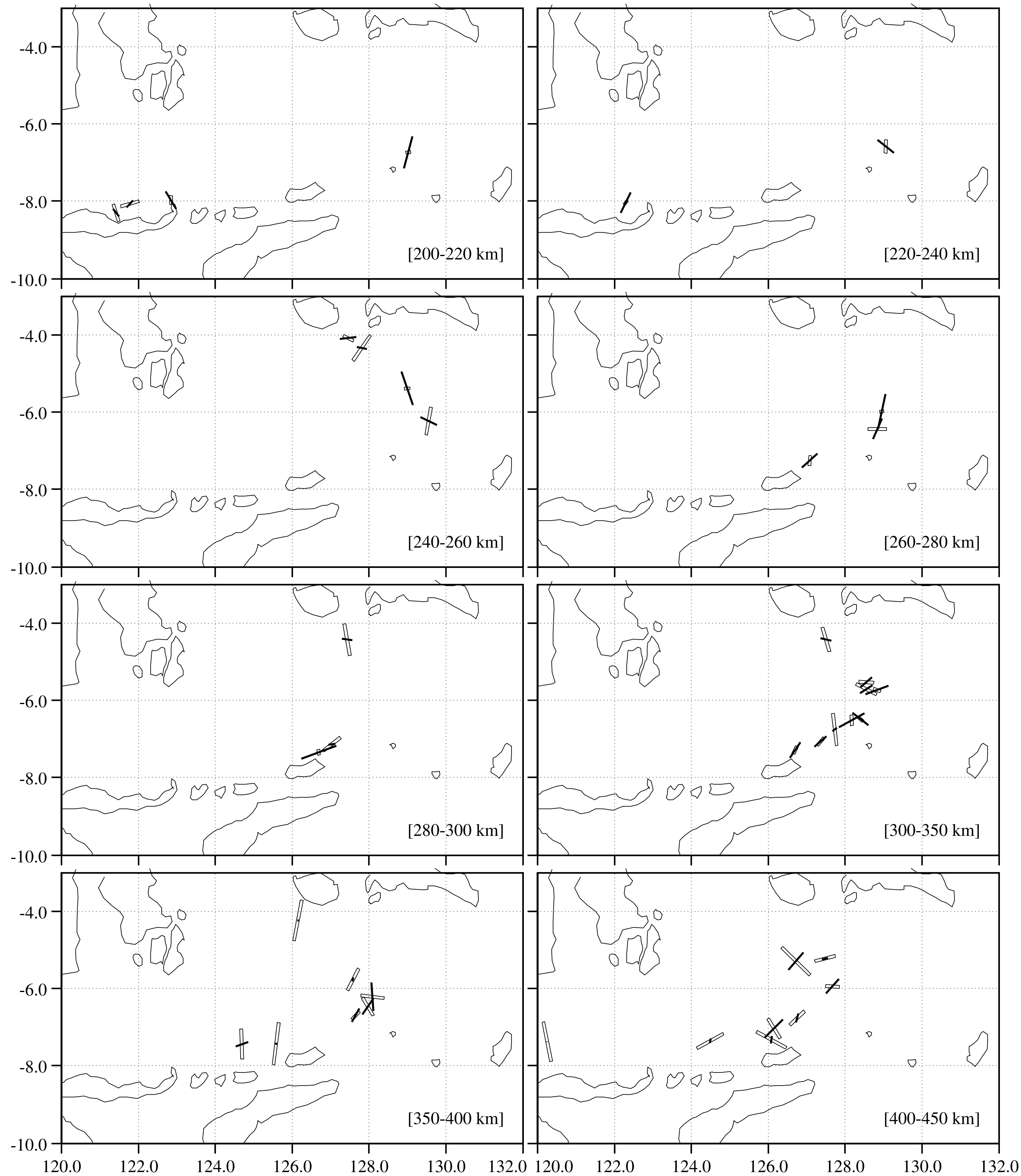

Figure 7b. Same as Figure 7a but for depth sections from 200 to 450 km depth.

encounters resistance to further penetration into the mantle near the 670 km boundary. The *P* axes of the relocated CMT earthquake at 100 km distance indicates N-S horizontal compression. Profile $\tau\tau'$ (Figure 6d) showed that the hypocentral locations of the earthquakes at 100 and 120 km distance in $\beta\beta'$ below 600 km closely follow the trend of the southwestward dipping Seram slab. The flattening of the slab near 600 km, seen in $\beta\beta'$, continues into $\gamma\gamma'$ to its east and has an upgoing portion to the right of the profile, forming a U shape, as reported by *McCaffrey* [1989]. This shows the convergence of the Flores-Timor part of the slab with the Seram slab.

[25] The deep Sulawesi earthquakes lie ~250–300 km to the north of the deepest part of the Flores-Timor WBZ (Figure 3a), and about the same distance to the west of the 400 km level of the Seram seismic zone (profile *oo*′ in Figure 6c). This profile shows that these Sulawesi earthquakes are consistent with being on the downdip extension

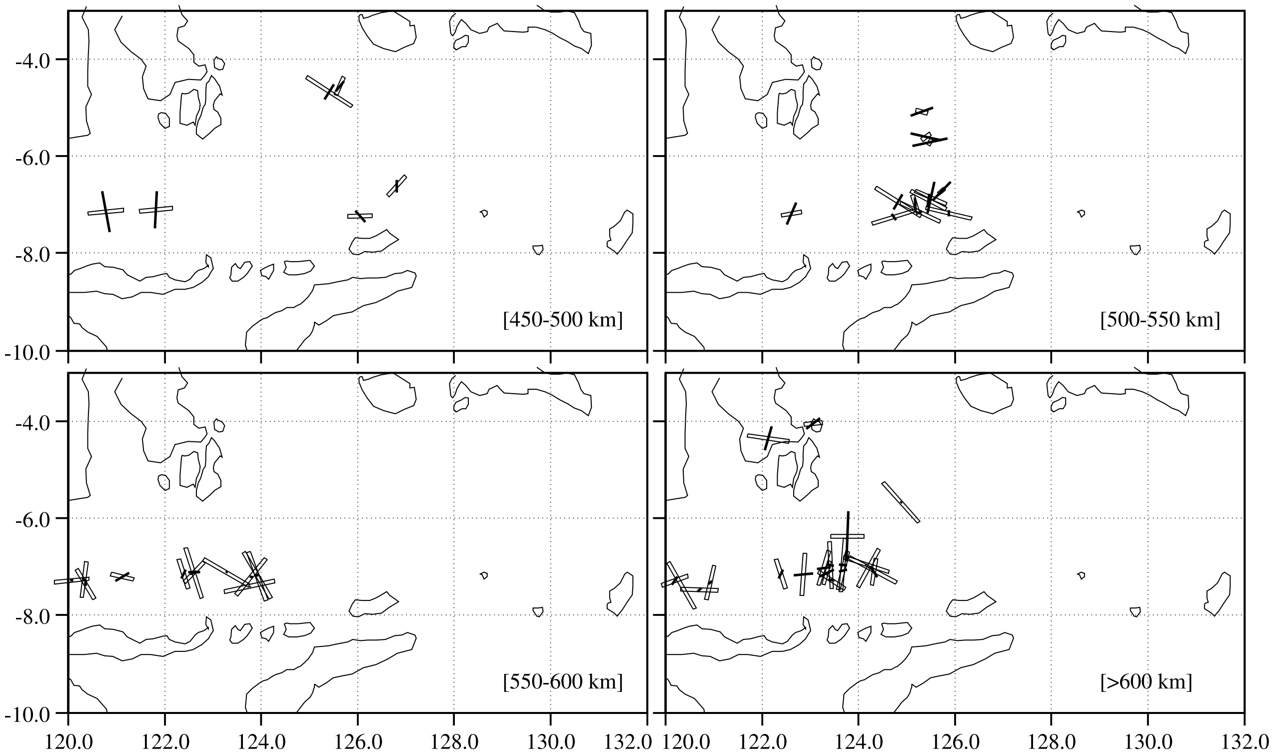

Figure 7c. Same as Figure 7a but for depth sections from 450 to >600 km depth.

of the structure defined by hypocenters to the east. On the other hand, in profiles $\alpha\alpha'$ and $\beta\beta'$, these earthquakes are clearly well off the FTT WBZ, and connecting these earthquakes with this WBZ, as was done by *Cardwell and Isacks* [1978] and *Lundgren and Giardini* [1994], is difficult. Nor is there any high seismic activity attesting to high stresses due to a sharp 90° bend in the WBZ at depth of about 600 km as would be required for this connection. Therefore we propose that these earthquakes occur at the lowest part of the WSW dipping Seram seismic zone, a conclusion different from previous studies. On the basis of this, we can now conclude that the Seram zone also extends down to below 600 km. Figure 8 shows a rough 3-D schematic of the Banda arc WBZ.

4.2. Two-Slab Model

[26] We conclude that our relocated earthquakes together with the *P* and *T* axes support the two-slab model. No tear (seismic gap) of the kind that would be required for the one-plate model [*Yamaoka et al.*, 1986] is seen along the seismic zone near 6°S, which has been examined from many angles by making 3-D plots (as in Figure 3b) from many directions (not plotted here). We saw the high activity on the FTT slab, which was under horizontal compression as it bends

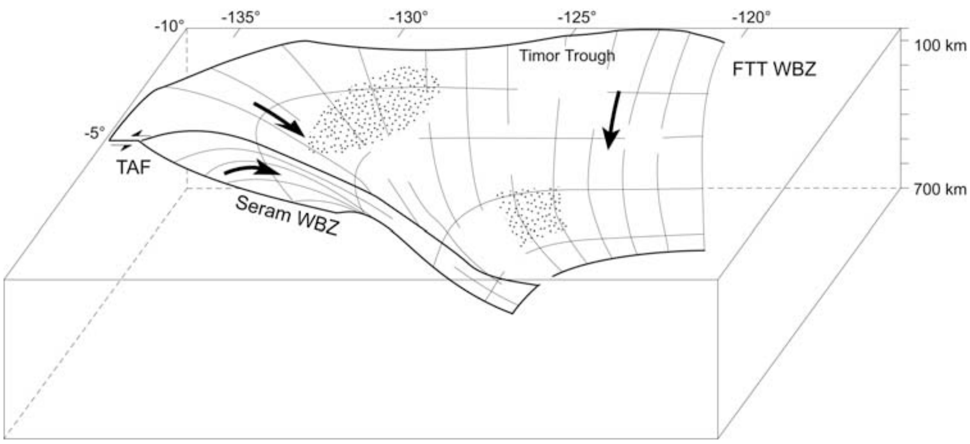

Figure 8. Rough three-dimensional view of the FTT and Seram WBZ. The approximate positions of the seismicity gaps of Table 1 are indicated by the missing grid lines on the WBZ. Regions of higher thickness are shown by stippling.

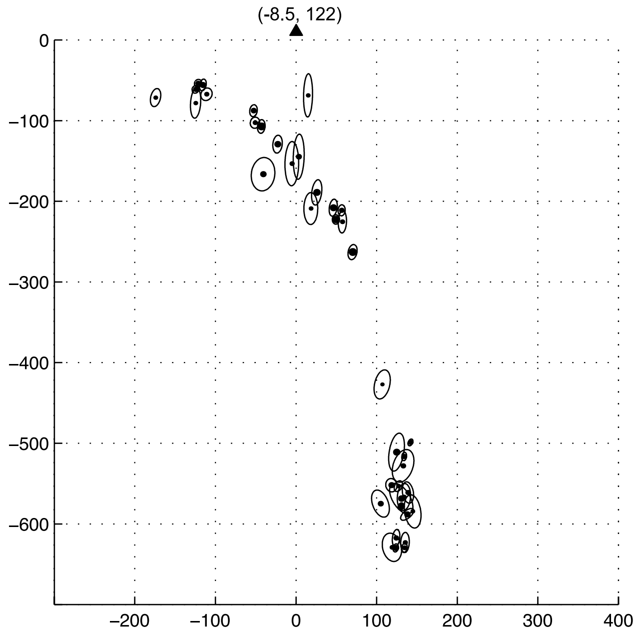

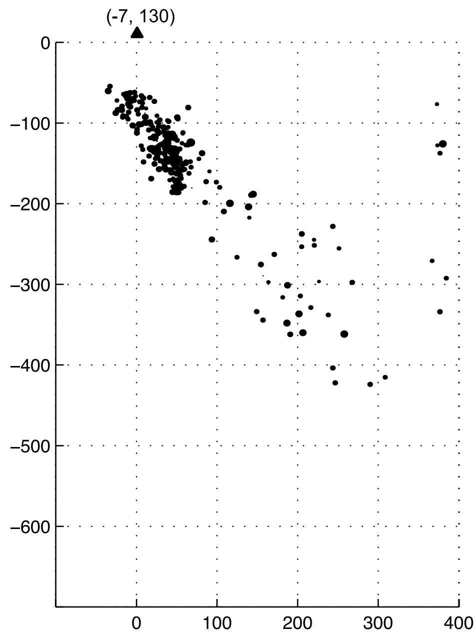

Figure 9. Two seismicity profiles, across the volcanoes (approximately shown by triangles, profiles include several volcanoes), to show depth of WBZ below the volcanoes. (top) A representative north-south profile, centered at (−8.5°, 122°), with a width of ±100 km about the center line, spanning the region between ∼121 and 123°E. The actual measurements were made using narrow profiles centered on each volcano (not shown). The error ellipsoids, projected on to the vertical plane, are shown and are representative of the errors for the profiles shown elsewhere in the paper. (bottom) Profile centered at (−7°, 130°). The profile is looked at from 40° west of north. Error ellipses not shown due to high seismicity.

northward near 130°E. If the entire arc were one slab, then we should have seen similarly high seismic activity near the sharper westward bend of the arc further north. This absence of seismicity provides additional support for the two-slab model. We identify the transition between the northward subducting Australian plate and the WSW subduction at the Seram trough to lie in the zone of the dashed line shown in Figure 3a, based on the sudden change in the level of seismicity across this linear zone. Thus the region of highest curvature has the highest seismic activity, suggesting increased stresses here. It is also the only part of the arc with seismicity continuously from the surface down to below 600 km. There seems to be no obvious reason why this line of transition also is the approximate westward extrapolation of the TAF along the slab, since according to the kinematic models of the region [*Cardwell and Isacks*, 1978; *McCaffrey*, 1988; *McCaffrey and Abers*, 1991], the TAF itself is not subducting.

[27] The FTT WBZ between about 127 and 131°E at depths between 100 and 200 km, just south of this transition line, is exceedingly thick. This could be either due to the folding over of the slab as it turns north around the arc here or due to some overlap between the two slabs. In fact, both could be occurring, since the WBZ is thickest closest to the Seram slab between 100 and 200 km depth here. Unfortunately, the hypocentral locations cannot separate the earthquakes in one slab from those in the other, and therefore we cannot say which slab lies above the other. However, with more data in future, it may be possible to resolve this.

4.3. Depth of Wadati-Benioff Zone Below the Arc Volcanoes

[28] By plotting many narrow seismicity profiles (not shown) through the arc volcanoes, we have measured the depth of the WBZ below these volcanoes. Two (wider) profiles are shown in Figure 9. We find that for the five volcanoes between 128 and 130°E, this depth lies in the ∼60–100 km depth range. For the 23 volcanoes between 118 and 124°E, the depth is ∼150 km. The former depth falls in the range obtained by *England et al.* [2003], but the latter well outside it. The WBZ on both regions dips at ∼50–55° directly below the volcanoes. The subduction rate for the former and latter arcs are ∼6 and ∼8 cm yr^{-1}, respectively. In every comparison of depth versus various parameters (dip of WBZ, rate of subduction, etc.), the 23 volcanoes between 118 and 124°E are extreme outliers, while the five volcanoes between 128 and 130°E fall in the middle of the range spanned by the data of *England et al.* [2003].

4.4. Implications for Intermediate and Deep Earthquake Mechanism

[29] This study shows that well located earthquakes over a long time period can reveal details of the seismic zone and associated slab not seen earlier. Such studies provide strong seismological constraints on possible mechanisms for the occurrence of intermediate and deep earthquakes [*Green and Burnley*, 1989; *Green et al.*, 1990; *Green*, 1994; *Kirby et al.*, 1996b; *Estabrook*, 2004]. For example, why are the depths of seismicity gaps so variable along the same arc? What causes abrupt

changes in the level of seismic activity and the thickness of the WBZ along an arc? Existing models often explain some observations but ignore others. For example, the suggestion that interaction of the descending slab with higher-viscosity material below 670 km leads to the globally observed seismicity distribution with depth [*Vassiliou and Hager*, 1988] explains the low number of earthquakes between 300 and 400 km depths but not the sudden increase near 500 km depth, nor the seismicity peak near 600 km depth [*Estabrook*, 2004]. The fact that the only part of the entire Indonesia and Banda arcs that has seismicity continuously from the surface to below 600 km is located at the region of the highest arc curvature suggests that the effect of slab stresses are the dominant factor along this arc. Increased stresses due to slab curvature and contortion can explain, for example, the increase of seismicity in some places, but less so the sudden decrease of seismicity in adjacent regions. One possible way to explain both the increased seismicity at some depths and decreased seismicity at other depths is by considering the effect of distributed heterogeneity within the slab. One special kind of heterogeneity, namely, the effect of preexisting faults has been considered previously [*Silver et al.*, 1995; *Kirby et al.*, 1996b], and fault heterogeneity is implicit in aftershock studies of subcrustal earthquakes [*Frohlich*, 1989, 1998; *Wiens and Gilbert*, 1996]. Thermokinetic models [see *Kirby et al.*, 1996b] which do explain many aspects of the broad features of observed seismicity distributions could be modified to take into account distributed slab heterogeneity. Changes in the thickness of the WBZ along the same arc could result from changes in the thermal regime due to increased stresses in the slab caused by its contortion and flexure. A similar mechanism may also explain seismically quiet zones adjacent to very active zones at the same depth. This again places constraints on models of subcrustal faulting.

[30] **Acknowledgments.** Hans Schöffel handpicked the phases from the seismograms, and was supported by the UK NERC studentship (GT4/96/234) and by the EC program, Environment and Climate, Topic IV.I.I, Natural Risks - Seismic Hazards, under Environment contract ENV4-CT 96-0296. I would like to thank Jim Dewey for use of his original JHD programs, and Chris Henry for use of his modified JHD programs. Discussions with Jim Dewey are gratefully acknowledged. An anonymous reviewer, Chuck Estabrook, and the Associate Editor Kelin Wang provided many constructive comments which improved the paper greatly, and their help is gratefully acknowledged. I would like to thank Dave Sansom and Dave Robinson for help with some of the figures.

References

Bird, P. (2003), An updated digital model of plate boundaries, *Geochem. Geophys. Geosyst.*, *4*, 1027, doi:10.1029/2001GC000252.

Bock, Y., L. Prawirodirdjo, J. F. Genrich, C. W. Stevens, R. McCaffrey, C. Subarya, S. S. O. Puntodewo, and E. Calais (2003), Crustal motion in Indonesia from Global Positioning System measurements, *J. Geophys. Res.*, *108*(B8), 2367, doi:10.1029/2001JB000324.

Bowin, C., G. M. Purdy, C. Johnston, G. Shor, L. Lawver, H. M. S. Hartono, and P. Jezek (1980), Arc-continent collision in the Banda Sea region, *AAPG Bull.*, *64*, 868–915.

Cardwell, R. K., and B. L. Isacks (1978), Geometry of the subducted lithosphere beneath the Banda Sea in eastern Indonesia from seismicity and fault plane solutions, *J. Geophys. Res.*, *83*, 2825–2838.

Das, S., and H.-J. Schöffel (2000), Accurate earthquake locations under Indonesia: Implications for Wadati-Benioff zone shape, mantle dynamics and deep earthquake mechanism, in *Problems in Geophysics for the New Millennium*, Compositori, Bologna, Italy, 47–72.

Das, S., H.-J. Schöffel, and F. Gilbert (2000), Mechanism of slab thickening and weakening near 670 km under Indonesia, *Geophys. Res. Lett.*, *27*, 831–834.

DeMets, C., R. G. Gordon, D. F. Argus, and S. Stein (1994), Effect of recent revisions to geomagnetic reversal time scale on estimates of current plate motions, *Geophys. Res. Lett.*, *21*, 2191–2194.

Dewey, J. W. (1971), Seismic studies with the method of joint hypocenter determination, Ph.D. thesis, Univ. of Calif., Berkeley.

Dewey, J. W. (1983), Relocation of instrumentally recorded pre-1974 earthquakes in the South Carolina region, in *Studies Related to the Charleston, South Carolina, Earthquake of 1886—Tectonics and Seismicity*, edited by G. S. Gohn, U.S. Geol. Surv. Prof. Pap., *1313*, Q1–Q9.

Dziewonski, A. M., et al. (1983–1999), Centroid-moment tensor solutions 1977–1998, *Phys. Earth Planet. Inter.*, *33–115*.

Engdahl, E. R., R. van der Hilst, and R. P. Buland (1998), Global teleseismic earthquake relocation with improved travel times and procedures for depth determination, *Bull Seismol. Soc. Am.*, *88*, 722–743.

England, P., E. R. Engdahl, and W. Thatcher (2003), Systematic variation in the depths of slabs beneath arc volcanoes, *Geophys. J. Intl.*, *156*, 377–408.

Estabrook, C. H. (2004), Seismic constraints on mechanisms of deep earthquake rupture, *J. Geophys. Res.*, *109*, B02306, doi:10.1029/2003JB002449.

Frohlich, C. (1989), The nature of deep-focus earthquakes, *Annu. Rev. Earth Planet. Sci.*, *17*, 227–254.

Frohlich, C. (1998), Does maximum earthquake size depend on focal depth?, *Bull. Seismol. Soc., Am.*, *88*, 329–336.

Genrich, J. F., Y. Bock, R. McCaffrey, E. Calais, C. W. Stevens, and C. Subarya (1996), Accretion of the southern Banda arc to the Australian plate margin determined by Global Positioning System measurements, *Tectonics*, *15*, 288–295.

Green, H. W., II (1994), Solving the paradox of deep earthquakes, *Sci. Am.*, *271*, 64–71.

Green, H. W., II, and P. C. Burnley (1989), A new self-organizing mechanism for deep-focus earthquakes, *Nature*, *341*, 733–737.

Green, H. W., II, T. E. Young, D. Walker, and C. H. Scholz (1990), Anticrack associated faulting at very high pressure in natural olivine, *Nature*, *348*, 720–722.

Hamilton, W. (1979), Tectonics of the Indonesian region, *U.S. Geol. Surv. Prof. Pap.*, *1078*, 345 pp.

Henry, C., and S. Das (2001), Aftershock zones of large shallow earthquakes: Fault dimensions, aftershock area expansion, and scaling relations, *Geophys. J. Int.*, *147*, 272–293.

Huang, W. C., E. A. Okal, G. Ekstrom, and M. P. Salganik (1997), Centroid-moment tensor solutions for deep earthquakes predating the digital era: The World-Wide Standardized Seismograph Network dataset (1962–1976), *Phys. Earth Planet. Inter.*, *99*, 121–129.

Isacks, B., and P. Molnar (1971), Distribution of stresses in the descending lithosphere from a global survey of focal mechanism solutions of mantle earthquakes, *Rev. Geophys.*, *9*, 103–174.

Katili, J. A. (1975), Volcanism and plate tectonics in the Indonesian island arcs, *Tectonophysics*, *26*, 165–188.

Kirby, S. H., E. R. Engdahl, and R. Denlinger (1996a), Intermediate-depth intraslab earthquakes and arc volcanoes as physical expressions of crustal and uppermost mantle metamorphism in subducting slabs, in *Subduction: Top to Bottom*, *Geophys. Monogr. Ser.*, vol. 96, edited by G. Bebout at al., pp. 195–214, Washington, D. C.

Kirby, S. H., S. Stein, E. A. Okal, and D. C. Rubie (1996b), Metastable mantle phase transformations and deep earthquakes in subducting oceanic lithosphere, *Rev. Geophys.*, *34*, 261–306.

Lemoine, A., R. Madariaga, and J. Campos (2002), Slab-pull and slab-push earthquakes in the Mexican, Chilean and Peruvian subduction zones, *Phys. Earth Planet. Inter.*, *132*, 157–175.

Lundgren, P., and D. Giardini (1994), Isolated deep earthquakes and the fate of subduction in the mantle, *J. Geophys. Res.*, *99*, 15,833–15,842.

McCaffrey, R. (1988), Active tectonics of the eastern Sunda and Banda Arcs, *J. Geophys. Res.*, *93*, 15,163–15,182.

McCaffrey, R. (1989), Seismological constraints and speculations on Banda Arc tectonics, *Neth. J. Sea Res.*, *24*, 141–152.

McCaffrey, R., and G. A. Abers (1991), Orogeny in arc-continent collision: The Banda Arc and western New Guinea Geology, *J. Geophys. Res.*, *19*, 563–566.

Pegler, G., and S. Das (1996), The 1987–92 Gulf of Alaska earthquakes, *Tectonophysics*, *57*, 111–136.

Pegler, G., and S. Das (1998), An enhanced image of the Pamir-Hindu Kush seismic zone obtained from relocated earthquake hypocenters, *Geophys. J. Int.*, *134*, 573–595.

Pegler, G., S. Das, and J. H. Woodhouse (1995), A seismological study of the eastern New Guinea and the western Solomon Sea regions and its tectonic implications, *Geophys. J. Int.*, *122*, 961–981.

Sandwell, D. T., and W. H. F. Smith (1997), Marine gravity anomaly from Geosat and ERS 1 satellite altimetry, *J. Geophys. Res.*, *102*, 10,039–10,054.

Schöffel, H.-J., and S. Das (1999), Fine details of the Wadati-Benioff zone under Indonesia and its geodynamic implications, *J. Geophys. Res.*, *104*, 13,101–13,114.

Silver, P. G., S. L. Beck, T. C. Wallace, C. Meade, S. C. Myers, D. E. James, and R. Kuehnel (1995), Rupture characteristics of the deep Bolivian earthquake of 9 June 1994 and the mechanism of deep-focus earthquakes, *Science*, *268*, 69–73.

Simkin, T., and L. Siebert (1994), *Volcanoes of the World*, 2nd ed., Geoscience Press, Tucson, Ariz., 368 pp.

Vassiliou, M. S., and B. H. Hager (1988), Subduction zone earthquakes and stress in slabs, *Pure Appl. Geophys.*, *128*, 574–624.

Widiyantoro, S., and R. van der Hilst (1997), Mantle structure beneath Indonesia inferred from high-resolution tomographic imaging, *Geophys. J. Int.*, *130*, 167–182.

Wiens, D. A., and H. J. Gilbert (1996), Effect of slab temperature on deep-earthquake aftershock productivity and magnitude-frequency relations, *Nature*, *384*, 153–156.

Yamaoka, K., Y. Fukao, and M. Kumazawa (1986), Spherical shell tectonics: Effects of sphericity and inextensibility on the geometry of the descending lithosphere, *Rev. Geophys.*, *24*, 27–53.

S. Das, Department of Earth Sciences, University of Oxford, Parks Road, Oxford OX1 3PR, UK. (das@earth.ox.ac.uk)

Figure 2. (a) Tectonic setting of the study region and adjacent areas, with gravity field from *Sandwell and Smith* [1997]. Solid arrows indicate plate velocity vectors from NUVEL-1A [*DeMets et al.*, 1994]. Arrows north of the Tarera-Aiduna Fault (TAF) represent the motion of the Pacific plate relative to the Eurasia plate; south of the TAF they indicate the motion of the Australia plate relative to Eurasia, all values being in cm yr^{-1}. WSW subduction of the Bird's Head block beneath the Seram trench, inferred from GPS data [*Bock at al.*, 2003], is shown by the open arrow. Black triangles indicate volcanoes, taken from *Simkin and Siebert* [1994]. Black lines with open triangles show thrust faults, dipping in the direction of the triangles. The black line with harpoons on either side shows the position of the TAF and the direction of relative movement across it [*Hamilton*, 1979]. FT, Flores Thrust; WT, Wetar Thrust; SBB, South Banda Basin; NBB, North Banda Basin; and WB, Weber Deep. (b) Seismicity of the study region for the period 1964–1996. ISC hypocenters with m_b > 4.5 for earthquakes deeper than 50 km are shown. Circles are color coded by depth, as shown in the key. The size of circle is proportional to the earthquake magnitude. When considering the many smaller earthquakes seen in the ISC seismicity, it must be kept in mind that it is difficult to obtain accurate magnitudes for earthquakes with m_b < 5. Black lines are faults shown in Figure 2a. The deep M_w 7.8 Flores earthquake of 17 June 1996 located at (−7.1, 122.6) at 586 km depth is clearly seen. It was the largest and deepest known earthquake in the entire Sunda and Banda regions.

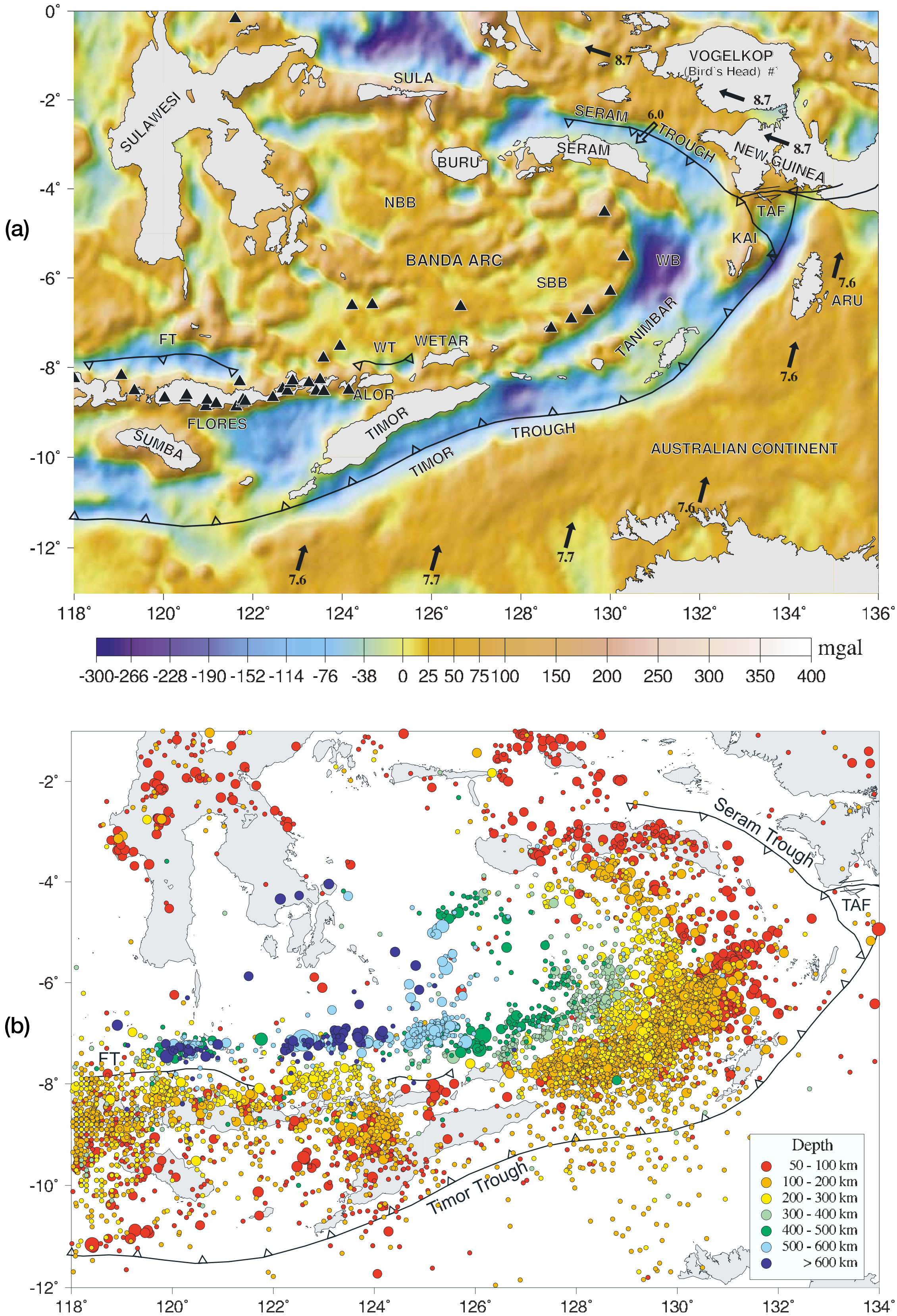
(a)
SULAWESI
SULA
VOGELKOP
(Bird's Head)
SERAM
TROUGH
NEW GUINEA
BURU
NBB
BANDA ARC
SBB
WB
TAF
KAI
ARU
TANIMBAR
FT
WT
WETAR
ALOR
FLORES
SUMBA
TIMOR
TROUGH
AUSTRALIAN CONTINENT
8.7
6.0
7.6
7.7
mgal
-300 -266 -228 -190 -152 -114 -76 -38 0 25 50 75 100 150 200 250 300 350 400
(b)
Seram Trough
TAF
FT
Timor Trough
Depth
50 - 100 km
100 - 200 km
200 - 300 km
300 - 400 km
400 - 500 km
500 - 600 km
> 600 km

Figure 2

Figure 3. (a) Map view of the relocated seismicity deeper than 50 km and with relocation error less than 30 km. Same color coding as in Figure 2b. Two CMT earthquakes from *Dziewonski et al.* [1983–1999] and *Huang et al.* [1997] are shown under southeast Sulawesi. Boxes show the positions of the profiles to be used in Figures 6a–6d. Solid black lines are faults, and the black triangles are volcanoes, as shown in Figure 2a. The dashed black line on the eastern part of the arc will be discussed in section 4.2. Arrows outside the frame show directions from which perspective plots are shown in Figure 3b. (b) (top) Perspective plots of the relocated seismicity, seen from two directions, 15° west of south and 5° north of east. (bottom) Seismicity on the FTT and Seram slabs, obtained by plotting earthquakes to the south and north of the 5°S latitude line. (This may not have separated the deep earthquakes where the slabs merge.) Colors, symbols, etc., are the same as in Figures 2b and 3a.

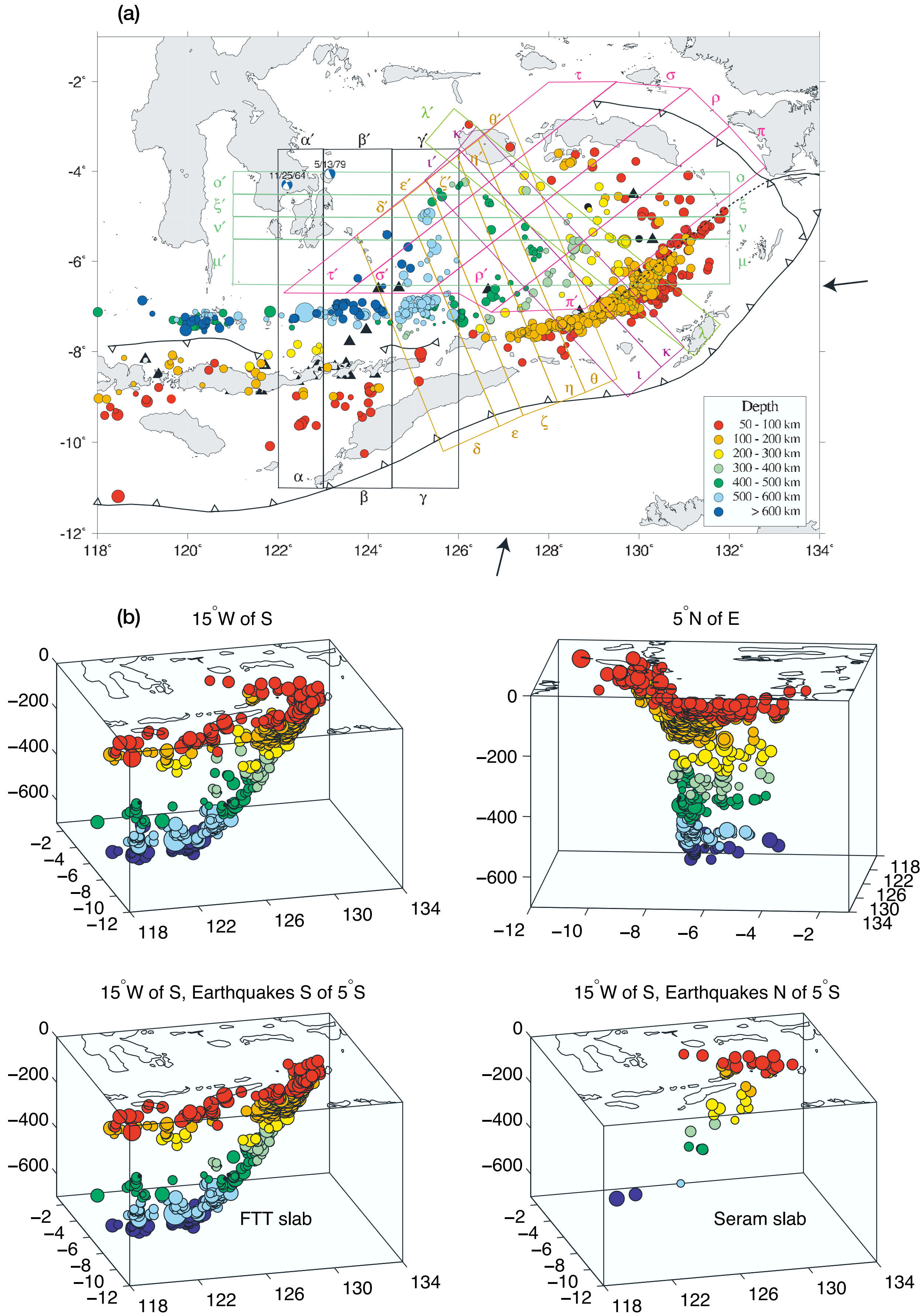
(a)
Depth
50 - 100 km
100 - 200 km
200 - 300 km
300 - 400 km
400 - 500 km
500 - 600 km
> 600 km
11/25/64
5/13/79
(b)
15°W of S
5°N of E
15°W of S, Earthquakes S of 5°S
15°W of S, Earthquakes N of 5°S
FTT slab
Seram slab

Figure 3

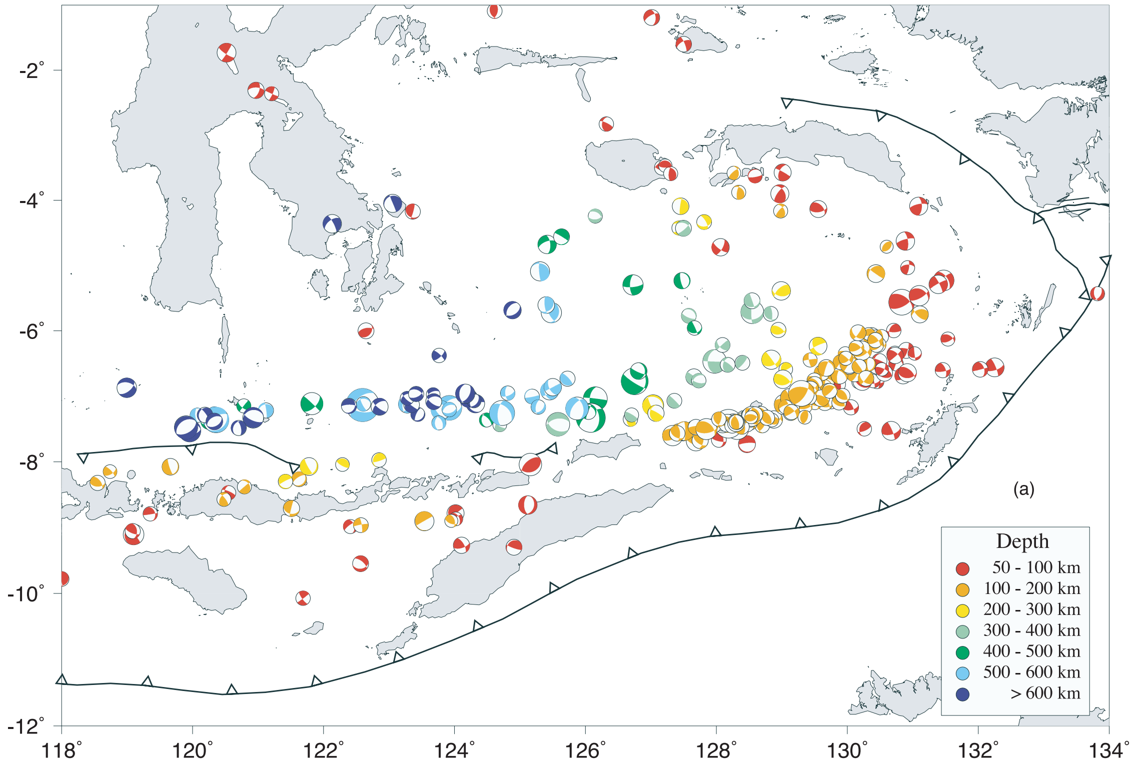

Figure 5. Same as Figure 4 but for earthquakes deeper than 50 km. CMTs are plotted at their relocated positions. The same color coding with depth as Figure 2b is used.

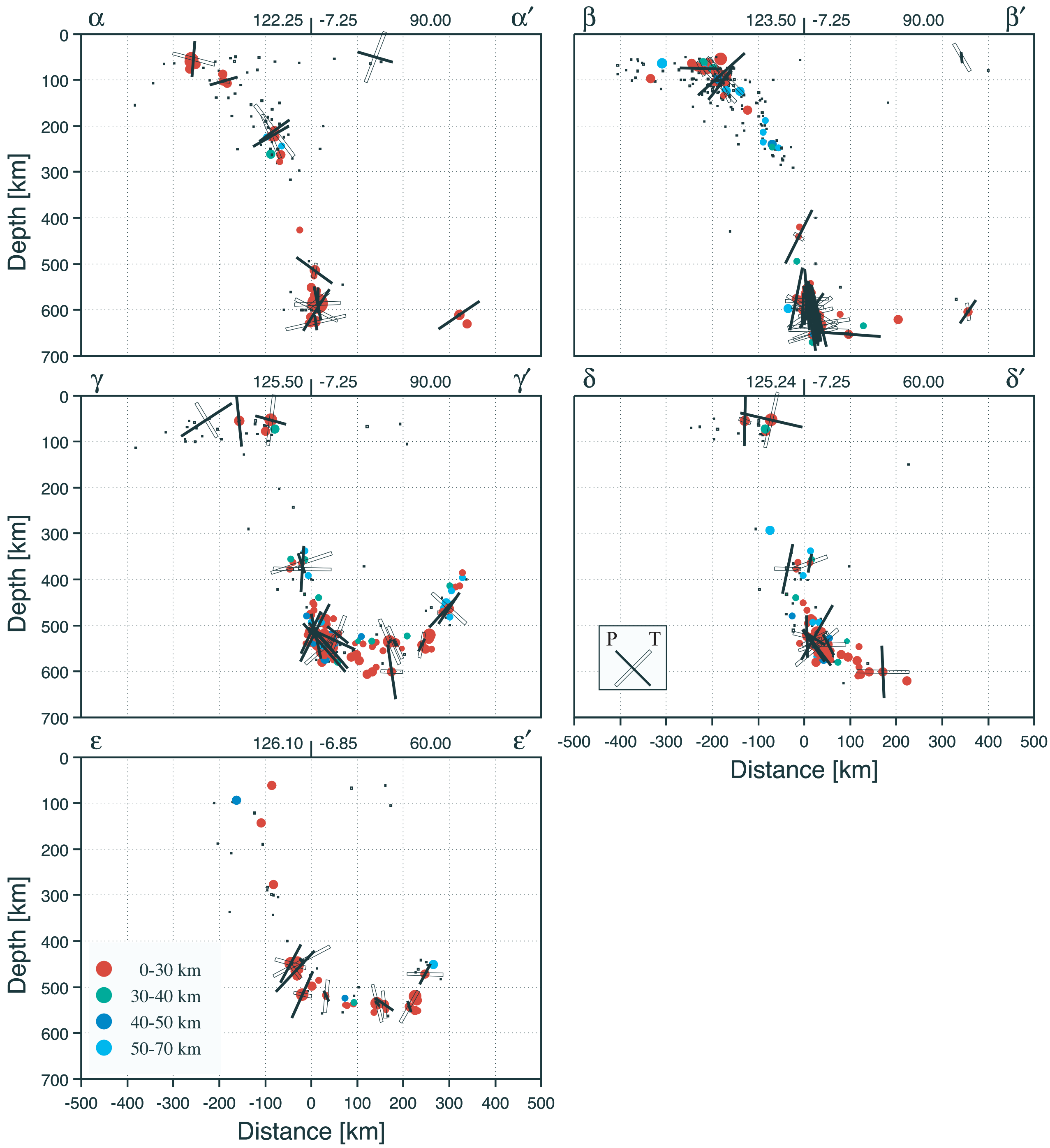

Figure 6a. Relocated seismicity profiles αα′ to εε′ (locations indicated in Figure 3a), projected onto the center line of the profile. Center position (longitude, latitude) and azimuth of the projection (e.g., 90° indicates profile is looked at from the east) are given on the top of each profile. The *P* and *T* axes of the CMT solution [*Dziewonski et al.*, 1983–1999; *Huang et al.*, 1997] are also shown. The different colored circles represent different maximum errors in the relocation, as shown in the color key. The *P* and *T* axes are projected into the plane of the profile and plotted at their relocated positions. Small open squares show the ISC seismicity with m_b > 4.0, which either could not be relocated or had a relocation error greater than 70 km. Symbols used for the *P* and *T* axes are shown.

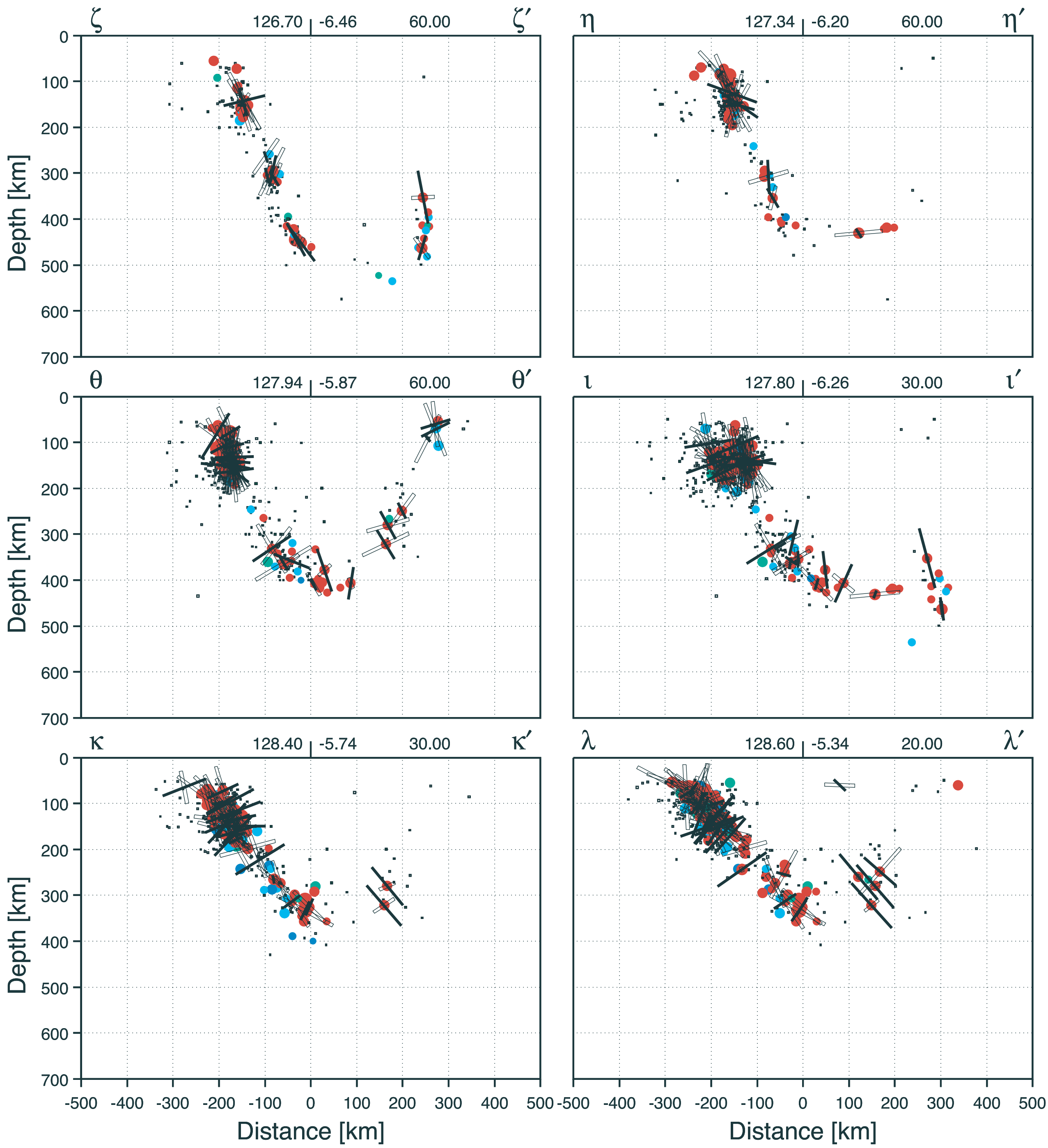

Figure 6b. Same as Figure 6a but for profiles ζζ′ to λλ′.

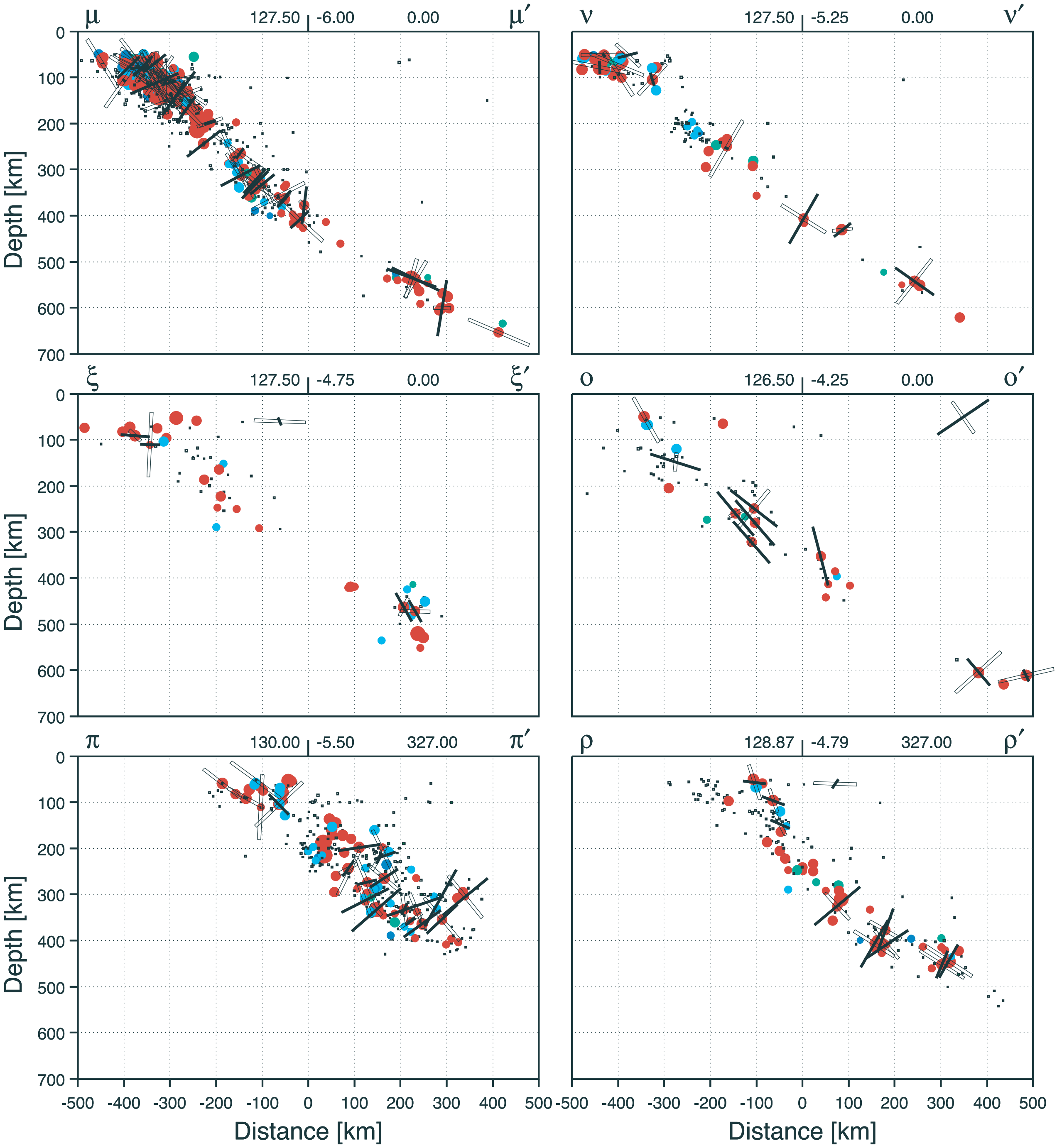

Figure 6c. Same as Figure 6a but for profiles μμ′ to ρρ′.

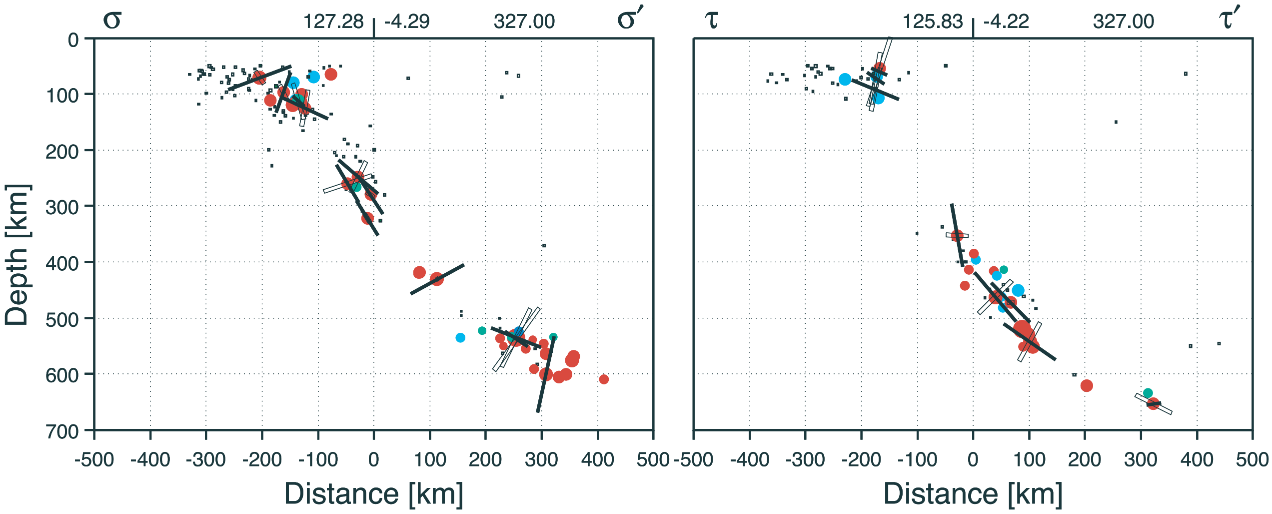

Figure 6d. Same as Figure 6a but for profiles σσ′ and ττ′.